European Journal of Mechanics / B Fluids 78 (2019) 88–105

Contents lists available at ScienceDirect

European Journal of Mechanics / B Fluids

journal homepage: www.elsevier.com/locate/ejmflu

Dispersion and attenuation in a porous viscoelastic model for gravity waves on an ice-covered ocean

Hua Chen [a], Robert P. Gilbert [a,b], Philippe Guyenne [a,*]

[a] Department of Mathematical Sciences, University of Delaware, DE 19716, USA
[b] Institute of Mechanics and Materials, Ruhr-Universität Bochum, Germany

ARTICLE INFO

Article history:
Received 15 February 2019
Received in revised form 1 June 2019
Accepted 5 June 2019
Available online 12 June 2019

Keywords:
Continuum model
Gravity waves
Poroelastic material
Sea ice
Viscoelasticity
Wave attenuation
Wave scattering

ABSTRACT

A two-dimensional continuum model is proposed for linear gravity waves propagating across ice-covered seas. It is based on a two-layer formulation where the floating sea ice is described as a homogeneous isotropic poroelastic material and the underlying ocean is viewed as a weakly compressible fluid. Dissipative effects are taken into account by including viscosity in rheological properties of the ice layer. An exact dispersion relation is derived for traveling wave solutions of this coupled system and numerical estimates are obtained for its complex roots. Extensive tests are conducted to examine the dependence of results on various parameters in both the porous and non-porous cases. Detailed comparison with existing viscoelastic models is provided, and good agreement on both wave dispersion and attenuation is found. In the porous case with friction, a non-monotonic behavior is observed for the attenuation rate as a function of frequency, which is reminiscent of the roll-over phenomenon that has been reported in field observations.

1. Introduction

1.1. Background

Major changes that have occurred in the polar regions over recent years such as the rapid decline of summer ice extent in the Arctic Ocean, have not been correctly predicted by modern climate models, suggesting that important physical components are missing. This has prompted a surge of research activity, and it is now recognized that ocean waves play an important role in controlling sea-ice morphology and in turn the presence of sea ice affects wave dynamics. These interactions are especially apparent in the marginal ice zone (MIZ), which is the fragmented part of the ice cover closest to the open ocean. As such, the MIZ is a highly heterogeneous and dynamic region, strongly affected by incoming waves. By breaking up the sea ice, waves cause it to become more fragmented, which in turn increases their capacity to further penetrate and damage the ice cover.

It is only recently that wave forecasting models have begun to be tested with parameterizations for wave-ice interactions. Of particular interest is the description of wave attenuation in the MIZ. Therefore, much effort has been devoted to developing parameterizations for the decay of wave energy due to sea ice, assuming an exponential behavior. Based on linear theory, two different approaches have been adopted: (i) separate-floe models where the ice cover is composed of individual floes with possibly different characteristics [1–3], and (ii) continuum models for waves propagating through a heterogeneous ice field described as a uniform material with effective rheological properties including viscosity or viscoelasticity [4–6]. Models of type (i) focus on wave attenuation by scattering, hence they are also referred to as wave-scattering models. Indeed, measurements from Wadhams et al. [7] provided evidence that wave scattering by ice floes is a dominant mechanism for energy attenuation in the MIZ. Predictions by this approach have recently been incorporated into operational wave forecasting models [8,9].

Models of type (ii) enable the direct (albeit tedious) calculation of an algebraic dispersion relation for traveling waves in the continuous medium. Wave scattering and other possible dissipative effects are encoded in the complex roots of this dispersion relation, and their relative importance is controlled by constant rheological parameters. These do not necessarily correspond to specific properties of sea ice but rather they are meant to represent effective properties of the ice field, similar to the way homogenized models characterize wave evolution in complex media [10,11]. While continuum models have been used for some time now, based mostly on thin-plate theory, to describe wave propagation in pack ice [12–14], it is only recently that they have been considered for application to the MIZ and for parameterization in operational wave forecasting models [15,16]. Recent popular models of type (ii) possess a high degree of sophistication

* Corresponding author.
E-mail addresses: chenhua@udel.edu (H. Chen), gilbert@udel.edu (R.P. Gilbert), guyenne@udel.edu (P. Guyenne).

https://doi.org/10.1016/j.euromechflu.2019.06.002
0997-7546/

and do not rely on the thin-plate assumption [6,17]. A more detailed review of this approach is given in the next section.

In this paper, we propose a two-dimensional continuum model for linear wave propagation in a coupled ice-ocean system, where the ice cover is viewed as a homogeneous isotropic poroelastic material. Viscosity can also be included in this formulation by allowing elasticity parameters to be complex numbers. A motivation for introducing such a model is that the porosity parameter may serve to provide a measure of ice concentration, which is an important quantity in sea-ice characterization. Using Biot's theory without the thin-plate assumption, we describe the heterogeneous ice field as a mixed layer with a solid phase and a fluid phase as the two limiting configurations. Aside from featuring porosity and viscoelasticity, our new model considers the fluid in both the floating ice layer and underlying ocean to be weakly compressible. The present work builds upon our ample experience with Biot's theory in the context of bone acoustics and ocean acoustics [18–22].

There is a large literature on the mathematical modeling and numerical simulation of ocean waves interacting with porous structures. In view are applications to coastal engineering where such structures are often used to dissipate wave energy for coastal protection. Examples include vertical breakwaters and floating or submerged horizontal plates; in particular the latter have drawn much attention recently because they do not block currents and do not hamper the seascape. Studies in this case often use the thin-plate approximation and focus on analyzing the performance of these structures in attenuating waves via scattering [23,24]. To our knowledge however, it is the first time here that a continuum model with porous viscoelastic features is introduced to describe wave propagation and attenuation in various types of ice cover, as possibly encountered in the MIZ.

After presenting the mathematical formulation, we derive an exact dispersion relation for surface wave solutions traveling in the horizontal direction. Given the complicated nature of this problem, involving a large number of physical parameters, we perform extensive tests of our Biot model in comparison with existing models in their respective limits. We solve this dispersion relation numerically and examine its predictions in both the porous and non-porous cases. As a byproduct of this study, we find that simpler viscoelastic models perform well overall, even in comparison with our predictions for nonzero porosity, displaying qualitatively similar properties of wave dispersion and attenuation. On the other hand, our Biot model is able to reproduce a non-monotonic behavior of the attenuation rate as a function of frequency, similar to the roll-over phenomenon that has been reported in field observations [7] but which has eluded linear scattering or viscoelastic models. In the context of our poroelastic formulation, this intriguing result is attributed to friction caused by the relative motion between the solid and fluid components, and thus is directly connected to the porous nature of the ice cover. Finally, exploiting the fact that porosity is represented by a small dimensionless parameter, we also propose an alternate version of the dispersion relation, based on a first-order Taylor expansion, which exhibits a more explicit dependence on this parameter.

1.2. Existing models

Recent reviews on continuum models for linear wave propagation across ice-infested seas can be found in [14,16,25,26]. We present here a brief overview of some of these models as they are relevant to our discussion in Section 3. They usually describe the underlying ocean by potential-flow theory for an ideal fluid (i.e. incompressible, inviscid and irrotational) [27]. In the absence of sea ice, the dispersion relation for surface traveling waves is given by

$$\omega^2 = gk\tanh(kH)\,, \tag{1}$$

where $\omega \in \mathbb{R}_+$ is the angular frequency, $k \in \mathbb{R}_+$ is the wavenumber, H is the (uniform) ocean depth and g is the acceleration due to gravity.

The simplest way to introduce sea-ice effects is by incorporating the added mass of ice at the water surface, which is known as the mass-loading (ML) model [25]. This changes (1) to

$$\frac{\omega^2}{g - A\,\omega^2} = k\tanh(kH)\,, \tag{2}$$

where $A = \theta\rho_s h/\rho_f$ represents ice inertia, θ is the fraction of surface area covered by ice, h is ice thickness, ρ_s and ρ_f are the densities of sea ice and water respectively. Because inertia appears as a negative term in the denominator of (2), mass loading tends to increase the wavenumber, i.e. it shortens the wavelength as compared to the ice-free case (1). It is suitable when the wavelength is much longer than the typical size of ice floes.

The mass-loading model ignores the elastic response of the ice cover. To overcome this deficiency, an alternate form

$$\frac{\omega^2}{g - A\,\omega^2 + L\,k^4/\rho_f} = k\tanh(kH)\,, \tag{3}$$

can be derived following Kirchhoff–Love plate theory [12]. The additional term depending on

$$L = \frac{\mu\,h^3}{6(1-\nu)}\,,$$

represents the flexural rigidity of sea ice, with μ and ν being the corresponding shear modulus and Poisson's ratio respectively. The relative contributions of inertial and elastic terms in the denominator of (3) determines whether the wavelength is shorter or longer. Unlike inertia, flexural rigidity (i.e. elasticity) tends to increase the wavelength. We will refer to (3) as the FS model.

As proposed in [5], a different approach treats the ice cover as a suspension of solid particles in water. Interaction among these ice particles and the associated friction lead to wave energy dissipation. Accordingly, the problem is described in terms of a two-layer system with a viscous fluid lying on top of an ideal fluid. This coupled system gives a dispersion relation for complex modes $\kappa = k + \mathrm{i}\,q$ where $q \in \mathbb{R}_+$ denotes the attenuation rate. More specifically, k refers to propagation modes while q is a measure of dissipation as the wave travels across the ice field.

Wang and Shen [6], hereafter referred to as WS, extended this approach to include elasticity in the upper layer. The ice cover is viewed as a homogeneous incompressible viscoelastic material according to Voigt's model. Via the effective viscosity parameter

$$\eta_c = \eta + \mathrm{i}\,\frac{\mu}{\rho_s\omega}\,,$$

the corresponding dispersion relation can be expressed as

$$\omega^2 = Wg\kappa\,\tanh(\kappa H)\,, \tag{4}$$

where

$$W = 1 + \frac{\rho_s N_3}{\rho_f N_4}\,,\quad N_1 = \sqrt{\kappa^2 - \mathrm{i}\frac{\omega}{\eta_c}}\,,\quad N_2 = \omega + 2\mathrm{i}\,\eta_c\kappa^2\,,$$

and

$$\begin{aligned} N_3 &= (g^2\kappa^2 - N_2^4 - 16\kappa^6 N_1^2\eta_c^4)\sinh(\kappa h)\sinh(N_1 h) \\ &\quad - 8\kappa^3 N_1\eta_c^2 N_2^2\big[\cosh(\kappa h)\cosh(N_1 h) - 1\big]\,, \\ N_4 &= g\kappa\big[4\kappa^3 N_1\eta_c^2\sinh(\kappa h)\cosh(N_1 h) + N_2^2\cosh(\kappa h)\cosh(N_1 h)\end{aligned}$$

$$-g\kappa \sinh(\kappa h)\sinh(N_1 h)\big]\,.$$

The parameter η denotes a kinematic viscosity associated with sea ice. Eq. (4) synthesizes the effects of an elastic plate and a viscous layer, and converges to their respective dispersion relations in appropriate limits.

A drawback of the WS model and its predecessor [5], the pure viscous layer model, is that multiple wave modes of complicated physical nature exist [28]. This has prompted Mosig et al. [26] to modify the FS model by introducing the complex Voigt shear modulus

$$\mu_c = -\mathrm{i}\,\rho_s\omega\eta_c = \mu - \mathrm{i}\,\omega\rho_s\eta\,. \tag{5}$$

The resulting dispersion relation (hereafter referred to as EFS) takes the form

$$\frac{\omega^2}{g - A\omega^2 + (B - \mathrm{i}\,C)\kappa^4} = \kappa\tanh(\kappa H)\,, \tag{6}$$

where

$$B = \frac{L}{\rho_f}\,, \quad C = \frac{\omega\rho_s\eta(1-\nu)h^3}{6\rho_f}\,.$$

This simpler viscoelastic model predicts fewer wave modes than (4), nonetheless it has been found to produce similar results for a wide range of parameter values, which also compare well to field observations.

It should be emphasized that Eqs. (3) and (6) represent thin-plate models while Eq. (4) corresponds to a layer model. The thin-plate approximation is typically valid when the wavelength is much longer than the ice thickness. This greatly simplifies the modeling in the sense that the ice cover is simply viewed as a boundary coinciding with the water surface, and sea-ice effects are taken into account via pressure terms there. By contrast, the present poroelastic model is based on a two-layer formulation in the spirit of WS.

The remainder of this paper is organized as follows. Section 2 presents the mathematical formulation of the coupled ice-ocean system, including the governing equations in each region as well as the coupling boundary conditions. Section 3 establishes the linear dispersion relation for surface traveling waves and provides a detailed parametric assessment in both the porous and non-porous cases, including comparisons with existing viscoelastic models. Finally, concluding remarks are given in Section 4.

2. Mathematical model

We describe here in detail our mathematical model for the coupled ice-ocean system. We restrict our attention to the two-dimensional case where the Cartesian coordinates (x, z) represent the horizontal and vertical directions, respectively. The z-axis points upward and the $z = 0$ level corresponds to the ice–water interface at rest (see Fig. 1). We assume all disturbances are small enough so that linear equations can be used for both the ice and water motions.

2.1. Equations for the underlying ocean

We consider an ocean of infinite extent in the x-direction and of constant depth H in the z-direction. The fluid (i.e. water) is assumed to be inviscid and weakly compressible, and the flow is irrotational. The fluid density $\rho = \rho_f + \widetilde{\rho}$ is viewed as the sum of a constant background density ρ_f and a perturbation $\widetilde{\rho}(x, z, t) \ll \rho_f$, where t denotes time. Taking the fluid to be barotropic [29], its pressure field can be Taylor expanded as

$$P(\rho) = P(\rho_f) + c^2\widetilde{\rho}\,, \tag{7}$$

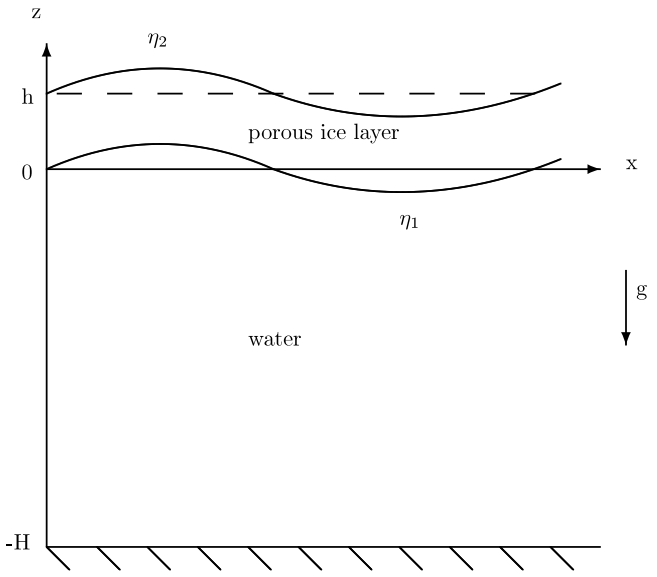

Fig. 1. Sketch of the coupled ice-ocean system.

where higher-order terms in $\widetilde{\rho}$ are neglected, and

$$c^2 = \left.\frac{\partial P}{\partial\rho}\right|_{\rho=\rho_f}\,,$$

defines the speed c of sound in water. The small compressibility of water is assumed here in order to be consistent with Biot's equations for the floating sea ice, as described in the next section. Flow irrotationality implies that there exists a velocity potential $\Phi(x, z, t)$ such that the fluid velocity $\mathbf{v}(x, z, t)$ satisfies $\mathbf{v} = \nabla\Phi$, where $\nabla = (\partial_x, \partial_z)$ is the spatial gradient. Similar to (7), inclusion of $\mathbf{v}$ should be viewed as a perturbation to the quiescent state.

To leading order, the equations for mass and momentum conservation read

$$\partial_t\widetilde{\rho} + \rho_f\nabla^2\Phi = 0\,, \tag{8}$$

and

$$\partial_t\Phi + \frac{P}{\rho_f} + g\,z = 0\,, \tag{9}$$

respectively. Combining (9) with (7) and (8) yields the wave equation

$$\partial_t^2\Phi - c^2\nabla^2\Phi = 0\,, \quad \text{for} \quad x\in\mathbb{R}\,,\ -H < z < 0\,. \tag{10}$$

There are two natural boundary conditions at the ocean surface, namely the kinematic condition

$$\partial_z\Phi = \partial_t\eta_1\,, \quad \text{at} \quad z = 0\,, \tag{11}$$

and the dynamic (Bernoulli's) condition

$$P = -\rho_f(\partial_t\Phi + g\,\eta_1)\,, \quad \text{at} \quad z = 0\,, \tag{12}$$

where $\eta_1(x, t)$ represents the vertical displacement of the ocean surface relative to $z = 0$. At the ocean floor, the impermeability condition amounts to

$$\partial_z\Phi = 0\,, \quad \text{at} \quad z = -H.$$

2.2. Equations for the floating sea ice

We consider an ice layer of infinite extent in the x-direction and of constant thickness h in the z-direction, lying on top of the ocean. Having the MIZ in mind, this ice layer is modeled by

Table 1
Parameters in Biot's equations: Notation, definition, typical value and SI units.

Symbol	Parameter	Value	Units
c	Sound speed in fluid part	1449	m s^{-1}
ρ_f	Density of fluid part	1025	kg m^{-3}
ρ_s	Density of solid part	917	kg m^{-3}
K_f	Bulk modulus of fluid part	1.1×10^5	Pa
K_s	Bulk modulus of solid part	4.3×10^5	Pa
μ	Shear modulus	2×10^5	Pa
K_c	Complex bulk modulus		Pa
μ_c	Complex shear modulus		Pa
η	Kinematic viscosity	0.01	m^2 s^{-1}
K_p	Permeability		m^2
a	Pore size		m
b	Friction		kg m^{-3} s^{-1}
ω	Angular frequency		s^{-1}
ν	Poisson's ratio	0.3	
α	Pore tortuosity	5	
β	Porosity		

Biot's equations for a homogeneous isotropic poroelastic material with constant effective parameters, which is meant to represent a heterogeneous ice field composed of icy and wet areas in various states, with pack ice (solid phase) and near-open water (fluid phase) being the two limiting configurations. Assumptions of homogeneity and isotropy have commonly been used in continuum models and are reasonable for the MIZ. Unlike several existing models in the literature, we *a priori* make no smallness assumption on the ice thickness. More details are provided below.

2.2.1. Stress–strain relations

Following Biot [30,31], the poroelastic medium is viewed as a mixture of an elastic material with an interstitial fluid. Let $\mathbf{u}(x,z,t) = (u,v)$ and $\mathbf{U}(x,z,t) = (U,V)$ denote respectively the solid and fluid displacement vectors at any point in this medium. We introduce the strain tensor

$$e_{xx} = \partial_x u\,,$$
$$e_{xz} = e_{zx} = \frac{1}{2}\left(\partial_z u + \partial_x v\right)\,,$$
$$e_{zz} = \partial_z v\,,$$

together with the solid and fluid dilatations

$$e = \nabla\cdot\mathbf{u} = \partial_x u + \partial_z v\,,$$
$$\epsilon = \nabla\cdot\mathbf{U} = \partial_x U + \partial_z V\,.$$

These two quantities gauge the medium's compressibility in each of the two phases. Under isotropic and plane-strain conditions, the constitutive laws relating stresses (σ_{ij}, s) to strains (e_{ij}, e, ϵ) are given by

$$\sigma_{ij} = (\lambda\, e + Q\,\epsilon)\,\delta_{ij} + 2\mu_c\, e_{ij}\,, \quad i,j = \{x,z\}\,, \tag{13}$$
$$s = Q\, e + R\,\epsilon\,, \tag{14}$$

for the solid and fluid parts respectively, where δ_{ij} is the Kronecker delta. The interstitial fluid is defined in such a way that it is only subject to normal (scalar) stress s. These equations involve a number of parameters: β is a measure of the medium's porosity (i.e. the fluid fraction in a representative area of the porous medium), λ together with the shear modulus μ_c are also called Lamé's coefficients and represent elasticity (or viscoelasticity), Q is of the nature of a coupling between the volume change of the solid part and that of the fluid part, and R is a measure of the pressure required to force a certain volume of fluid into the aggregate. For a vast fragmented ice cover such as the MIZ, it is reasonable to assume that areas of open water (as seen on surface images) contribute to the medium's porosity.

Given β, μ and other quantities as described in Table 1, these parameters may be estimated by the following formulas

$$\lambda = K_c - \frac{2}{3}\mu_c + \frac{\left[(1-\beta)K_s - K_c\right]^2}{D - K_c}\,,$$
$$Q = \frac{\beta K_s\left[(1-\beta)K_s - K_c\right]}{D - K_c}\,,$$
$$R = \frac{\beta^2 K_s^2}{D - K_c}\,,$$

where

$$D = K_s\left[1 + \beta\left(\frac{K_s}{K_f} - 1\right)\right]\,,$$
$$K_s = \frac{2\mu\,(1+\nu)}{3(1-2\nu)}\,.$$

The bulk and shear moduli, K_c and μ_c, often admit imaginary parts to account for viscous dissipation in the bulk of each of the two phases. The bulk modulus may be estimated by

$$K_c = \frac{2\mu_c\,(1+\nu)}{3(1-2\nu)}(1-\beta)^n\,,$$

where μ_c would be given by (5) and $n = 1.4$ [20,22]. Therefore, if μ_c is complex, so is K_c (and so are λ, Q, R since they all depend on K_c). Note that the porosity β is a dimensionless parameter whose range is $0 \le \beta \le 1$. For reasons explained below, its limiting values $\beta = 0$ and $\beta = 1$ correspond to two different states that we refer to as "solid" and "fluid" respectively. In the present context, its complement $1-\beta$ may be viewed as a measure of ice concentration in the ice field (i.e. the fraction of ice-covered surface), and thus may be connected to the level of heterogeneity of the ice cover. Such a parameter is not present in existing viscoelastic models for wave propagation across ice-infested seas.

The total effective stress acting at any point in this poroelastic material can thus be expressed as

$$\tau_{ij} = \sigma_{ij} + s\,\delta_{ij}\,, \tag{15}$$

or more explicitly

$$\tau_{ij} = (M\, e + N\,\epsilon)\,\delta_{ij} + 2\mu_c\, e_{ij},$$

where

$$M = \frac{K_c\left[K_f(3K_s - 2\mu_c) - 3K_s^2\beta\right] + K_s\left[K_f(-1+\beta)(3K_s - 2\mu_c) + 2K_s\beta\mu_c\right]}{3K_cK_f - 3K_s\left[K_f(1-\beta) + K_s\beta\right]}\,,$$
$$N = \frac{K_f(K_c - K_s)K_s\beta}{K_cK_f - K_s\left[K_f(1-\beta) + K_s\beta\right]}\,,$$

by virtue of (13) and (14).

It can be checked that, as $\beta \to 0$ (assuming K_c and μ_c are real),

$$K_c \to K_s\,, \quad M \to K_s - \frac{2}{3}\mu\,, \quad N \to 0,$$

and Eq. (15) simplifies to

$$\tau_{ij} = \left(K_s - \frac{2}{3}\mu\right)e\,\delta_{ij} + 2\mu\, e_{ij},$$

which is the typical stress–strain relation for an isotropic elastic material. Note that it only involves the solid strain tensor together with μ and K_s while K_f is absent. Having the MIZ in mind, this limiting case would correspond to a solid ice pack. Compression and stretching of the ice layer are still allowed in this limit via the solid dilatation e, which contrasts with the EFS and WS models where such effects are neglected.

On the other hand, as $\beta \to 1$,

$$K_c \to 0\,, \quad M \to -\frac{2}{3}\mu\,, \quad N \to K_f\,,$$

and Eq. (15) reduces to

$$\tau_{ij} = \left(K_f\,\epsilon - \frac{2}{3}\mu\, e\right)\delta_{ij} + 2\mu\, e_{ij},$$

which involves the fluid dilatation ϵ together with K_f while K_s is absent. Although it is tempting to interpret this "fluid" limit as equivalent to the open ocean, the presence of additional terms containing the solid strain tensor (associated with the parameter μ) suggests a slightly different situation. According to Biot's theory, a porous material in this limit is viewed as an elastic frame that is fully saturated with fluid. In the present context, this may be interpreted as an ice cover that has reached an advanced stage of melting.

2.2.2. Equations of motion

Including gravity $\mathbf{g} = (0, -g)$ as an external body force, Biot's equations for the ice-layer dynamics read

$$\mu_c\,\nabla^2\mathbf{u} + \nabla\big[(\lambda+\mu_c)\,e + Q\,\epsilon\big] + \mathbf{F}_s = \partial_t^2(\rho_{11}\mathbf{u} + \rho_{12}\mathbf{U}) + b\,\partial_t(\mathbf{u}-\mathbf{U}), \tag{16}$$

$$\nabla(Q\,e + R\,\epsilon) + \mathbf{F}_f = \partial_t^2(\rho_{12}\mathbf{u} + \rho_{22}\mathbf{U}) - b\,\partial_t(\mathbf{u}-\mathbf{U}), \tag{17}$$

where

$$\mathbf{F}_s = (1-\beta)\rho_s\mathbf{g} = (0, F_s) = \big(0, -(1-\beta)\rho_s g\big),$$
$$\mathbf{F}_f = \beta\rho_f\mathbf{g} = (0, F_f) = (0, -\beta\rho_f g).$$

Terms involving the parameter b account for friction due to the relative motion between the fluid and solid parts. This parameter is related to Darcy's coefficient of permeability K_p by

$$b = \frac{\rho_s\eta\beta^2}{K_p}. \tag{18}$$

The coefficients ρ_{11} and ρ_{22} are density parameters associated with the solid and fluid parts respectively, while ρ_{12} is a density coupling parameter with a negative value. These are calculated from the following formulas

$$\rho_{11} = (1-\beta)\rho_s - \rho_{12},$$
$$\rho_{22} = \beta\rho_f - \rho_{12},$$
$$\rho_{12} = \beta(1-\alpha)\rho_f,$$

where the dimensionless parameter α is a measure of pore tortuosity in the ice layer [32].

Following Stoll and Kan [33], we now introduce the displacement potentials (Φ_s, Ψ_s) and (Φ_f, Ψ_f) such that $\mathbf{u}$ and $\mathbf{U}$ are decomposed into

$$u = \partial_x\Phi_s - \partial_z\Psi_s, \quad v = \partial_z\Phi_s + \partial_x\Psi_s,$$

$$U = \partial_x\Phi_f - \partial_z\Psi_f, \quad V = \partial_z\Phi_f + \partial_x\Psi_f,$$

with an irrotational part involving (Φ_s, Φ_f) and a rotational part involving (Ψ_s, Ψ_f). Eqs. (16) and (17) then become

$$(\lambda+2\mu_c)\nabla^2\Phi_s + Q\,\nabla^2\Phi_f = \partial_t^2(\rho_{11}\Phi_s + \rho_{12}\Phi_f) + b\,\partial_t(\Phi_s - \Phi_f),$$
$$Q\,\nabla^2\Phi_s + R\,\nabla^2\Phi_f = \partial_t^2(\rho_{12}\Phi_s + \rho_{22}\Phi_f) - b\,\partial_t(\Phi_s - \Phi_f),$$

and

$$\mu_c\,\nabla^2\Psi_s = \partial_t^2(\rho_{11}\Psi_s + \rho_{12}\Psi_f) + b\,\partial_t(\Psi_s - \Psi_f),$$
$$0 = \partial_t^2(\rho_{12}\Psi_s + \rho_{22}\Psi_f) - b\,\partial_t(\Psi_s - \Psi_f).$$

Note that the gravity terms in (16)–(17) are constants and thus may be ignored because they may be absorbed into the definition of the displacement potentials, as commonly done in potential-flow theory. These gravity terms however appear explicitly in boundary conditions as described below.

2.2.3. Traveling wave solutions

We restrict our attention to wave solutions of the form

$$(\Phi_s, \Phi_f, \Psi_s, \Psi_f) = \big[\phi_s(z), \phi_f(z), \psi_s(z), \psi_f(z)\big]e^{\mathrm{i}(\kappa x - \omega t)}, \tag{19}$$

traveling steadily in the x-direction. Under this assumption, the above equations reduce to

$$\nabla^2\big[(\lambda+2\mu_c)\,\phi_s + Q\,\phi_f\big] + p_{11}\phi_s + p_{12}\phi_f = 0,$$
$$\nabla^2(Q\,\phi_s + R\,\phi_f) + p_{12}\phi_s + p_{22}\phi_f = 0,$$

and

$$\mu_c\,\nabla^2\psi_s + p_{11}\psi_s + p_{12}\psi_f = 0, \tag{20}$$
$$p_{12}\psi_s + p_{22}\psi_f = 0, \tag{21}$$

where

$$p_{11} = \omega^2\rho_{11} + \mathrm{i}\,\omega\,b, \quad p_{12} = \omega^2\rho_{12} - \mathrm{i}\,\omega\,b, \quad p_{22} = \omega^2\rho_{22} + \mathrm{i}\,\omega\,b.$$

Then making the change of variables

$$\tau = (\lambda+2\mu_c)\,\phi_s + Q\,\phi_f, \quad \sigma = Q\,\phi_s + R\,\phi_f, \tag{22}$$

as in [19], such that

$$\phi_s = a_{11}\tau - a_{12}\sigma, \quad \phi_f = -a_{12}\tau + a_{22}\sigma, \tag{23}$$

with

$$a_{11} = \frac{R}{d}, \quad a_{12} = \frac{Q}{d}, \quad a_{22} = \frac{\lambda+2\mu_c}{d},$$

and

$$d = (\lambda+2\mu_c)R - Q^2,$$

yields

$$\nabla^2\tau + B_{11}\tau + B_{12}\sigma = 0, \tag{24}$$
$$\nabla^2\sigma + B_{21}\tau + B_{22}\sigma = 0, \tag{25}$$

where

$$B_{11} = a_{11}p_{11} - a_{12}p_{12}, \quad B_{12} = -a_{12}p_{11} + a_{22}p_{12},$$

$$B_{21} = a_{11}p_{12} - a_{12}p_{22}, \quad B_{22} = -a_{12}p_{12} + a_{22}p_{22}.$$

Taking the Laplacian of (24) and (25), we obtain the two decoupled equations

$$\Delta^2\tau + (B_{11}+B_{22})\Delta\tau + (B_{11}B_{22} - B_{12}B_{21})\,\tau = 0,$$
$$\Delta^2\sigma + (B_{11}+B_{22})\Delta\sigma + (B_{11}B_{22} - B_{12}B_{21})\,\sigma = 0,$$

and substituting the biharmonic operator Δ^2 with

$$\Delta^2 = (\nabla^2)^2 = (-\kappa^2 + \partial_z^2)^2 = \kappa^4 - 2\kappa^2\partial_z^2 + \partial_z^4,$$

by virtue of (19), we arrive at the fourth-order ordinary differential equation

$$\tau'''' + (B_{11}+B_{22}-2\kappa^2)\tau'' + \big[\kappa^4 - \kappa^2(B_{11}+B_{22}) + B_{11}B_{22} - B_{12}B_{21}\big]\tau = 0,$$

for τ, where the primes denote differentiation with respect to z.

The same equation governs σ and its general solution can be written as

$$\tau(z) = C_1\cosh(D_1 z) + C_2\sinh(D_1 z) + C_3\cosh(D_2 z) + C_4\sinh(D_2 z), \tag{26}$$

in terms of

$$D_1 = \sqrt{-\frac{F_1 + \sqrt{F_1^2 - 4F_2}}{2}}, \quad D_2 = \sqrt{-\frac{F_1 - \sqrt{F_1^2 - 4F_2}}{2}},$$

$$F_1 = B_{11} + B_{22} - 2\kappa^2,$$

$$F_2 = \kappa^4 - \kappa^2(B_{11} + B_{22}) + B_{11}B_{22} - B_{12}B_{21}\,.$$

It follows from (24) that

$$\sigma = -\frac{1}{B_{12}}\Delta\tau - \frac{B_{11}}{B_{12}}\tau = \frac{\kappa^2 - B_{11}}{B_{12}}\tau - \frac{1}{B_{12}}\tau''\,,$$

hence

$$\sigma(z) = C_1F_3\cosh(D_1z) + C_2F_3\sinh(D_1z) + C_3F_4\cosh(D_2z) + C_4F_4\sinh(D_2z)\,, \tag{27}$$

where

$$F_3 = -\frac{B_{11} + D_1^2 - \kappa^2}{B_{12}}\,, \quad F_4 = -\frac{B_{11} + D_2^2 - \kappa^2}{B_{12}}\,.$$

We are now in a position to recover the displacement potentials. Combining (23), (26) and (27) gives

$$\begin{aligned}\phi_s(z) &= C_1F_5\cosh(D_1z) + C_2F_5\sinh(D_1z) + C_3F_6\cosh(D_2z)\\ &\quad + C_4F_6\sinh(D_2z)\,,\\ \phi_f(z) &= C_1F_7\cosh(D_1z) + C_2F_7\sinh(D_1z) + C_3F_8\cosh(D_2z)\\ &\quad + C_4F_8\sinh(D_2z)\,,\end{aligned}$$

with

$$F_5 = a_{11} - a_{12}F_3\,, \quad F_6 = a_{11} - a_{12}F_4\,,$$

$$F_7 = -a_{12} + a_{22}F_3\,, \quad F_8 = -a_{12} + a_{22}F_4.$$

From (21), we deduce

$$\psi_f = -\frac{p_{12}}{p_{22}}\psi_s,$$

and substituting it into (20), we find

$$\psi_s'' - \left(\kappa^2 - \frac{p_{11}p_{22} - p_{12}^2}{p_{22}\mu_c}\right)\psi_s = 0.$$

Solving this equation leads to

$$\begin{aligned}\psi_s(z) &= C_5\cosh(D_3z) + C_6\sinh(D_3z)\,,\\ \psi_f(z) &= C_5F_9\cosh(D_3z) + C_6F_9\sinh(D_3z)\,,\end{aligned}$$

in which

$$D_3 = \sqrt{\kappa^2 - \frac{p_{11}p_{22} - p_{12}^2}{p_{22}\mu_c}}\,, \quad F_9 = -\frac{p_{12}}{p_{22}}.$$

Note that, for traveling wave solutions (19), the displacement and velocity fields play the same role because their expressions only differ by a constant factor. Accordingly, consideration of the fluid dilatation $\epsilon = \nabla\cdot\mathbf{U} \neq 0$ (i.e. the fluid displacement or velocity field is not divergence-free) together with the underlying linear approximation implies that the pore fluid is viewed as weakly compressible.

2.3. Boundary conditions for the coupled system

After presenting the individual models for the underlying ocean and floating ice layer, we can set up the coupled system by prescribing its boundary conditions, including the transmission conditions at the interface between these two regions. We assume the ocean surface and the bottom boundary of the ice layer coincide and there is no cavitation. As a consequence, these two boundaries bend in unison and, if we also look for traveling wave solutions of the form

$$\Phi(x, z, t) = \phi(z)\,e^{\mathrm{i}(\kappa x - \omega t)},$$

in the ocean, the wave equation (10) becomes

$$\phi'' - \left(\kappa^2 - \frac{\omega^2}{c^2}\right)\phi = 0\,, \tag{28}$$

whose general solution is

$$\phi(z) = C_7\cosh(D_4z) + C_8\sinh(D_4z),$$

with

$$D_4 = \sqrt{\kappa^2 - \frac{\omega^2}{c^2}}.$$

Technically speaking, we could possibly treat the ocean as an incompressible irrotational fluid, in which case the bulk equation for Φ would simply be Laplace's equation $\nabla^2\Phi = 0$, yielding $\phi'' - \kappa^2\phi = 0$, rather than (28), for traveling wave solutions. Because we end up either way with a second-order ordinary differential equation for ϕ, it did not cost us much more to consider the compressible case.

Since the resulting coupled system has eight unknowns C_i $(i = 1, \ldots, 8)$ in total, eight boundary conditions are required. These boundaries include the air–ice interface at $z = h$, the ice–water interface at $z = 0$ and the ocean floor at $z = -H$, therefore various boundary conditions come into play. In particular, because water in the ocean is taken to be inviscid, it does not exert any tangential stress on the ice layer. On the other hand, the dynamic condition at the ice–water interface implies that the ice normal stress should match the water pressure. The situation is complicated here by the fact that the ice layer is modeled as a poroelastic material.

Let $\eta_2(x, t) = \eta_1(x, t) + h$ denote the vertical displacement of the top boundary of the ice layer relative to $z = 0$. We specify the following boundary conditions:

- at the air–ice interface $z = h$
  1. vanishing of tangential stress $(\sigma_{xz} = \sigma_{zx} = 0)$

     $\partial_z u + \partial_x v = 0,$
  2. vanishing of solid normal stress $(\sigma_{zz} - F_s\eta_2 = 0)$

     $\lambda\, e + Q\,\epsilon + 2\mu_c\, e_{zz} + (1-\beta)\rho_s g\,\eta_2 = 0,$
  3. vanishing of fluid normal stress $(s - F_f\eta_2 = 0)$

     $Q\, e + R\,\epsilon + \beta\rho_f g\,\eta_2 = 0,$
- at the ice–water interface $z = 0$
  4. continuity of vertical displacement

     $(1-\beta)\, v + \beta\, V = \eta_1,$
  5. vanishing of tangential stress $(\sigma_{xz} = \sigma_{zx} = 0)$

     $\partial_z u + \partial_x v = 0,$
  6. continuity of solid normal stress $(\sigma_{zz} - F_s\eta_1 = -(1-\beta)P)$

     $\lambda\, e + Q\,\epsilon + 2\mu_c\, e_{zz} + (1-\beta)\rho_s g\,\eta_1 = -(1-\beta)P,$
  7. continuity of fluid normal stress $(s - F_f\eta_1 = -\beta P)$

     $Q\, e + R\,\epsilon + \beta\rho_f g\,\eta_1 = -\beta P,$
- at the ocean floor $z = -H$
  8. vanishing of fluid flux

     $\partial_z\Phi = 0.$

Information on η_1 and η_2 as required in conditions 2, 3, 6 and 7 is given by the kinematic condition (11). After η_1 has been determined, η_2 readily follows. As for P which is used in conditions 6 and 7, it is given by the dynamic condition (12).

More explicitly, in terms of the potentials for traveling wave solutions, these boundary conditions read:

- at the air–ice interface $z = h$

$$(\mathrm{i}\kappa\,\phi_s - \psi_s')' + \mathrm{i}\kappa\,(\phi_s' + \mathrm{i}\kappa\,\psi_s) = 0\,,$$
$$-\mathrm{i}\,\omega\big[\lambda\,\nabla^2\phi_s + Q\,\nabla^2\phi_f + 2\mu_c\,(\phi_s' + \mathrm{i}\kappa\,\psi_s)'\big] + (1-\beta)\rho_s g\,\phi' = 0\,,$$
$$-\mathrm{i}\,\omega\,(Q\,\nabla^2\phi_s + R\,\nabla^2\phi_f) + \beta\rho_f g\,\phi' = 0\,,$$

- at the ice–water interface $z = 0$

$$-\mathrm{i}\,\omega\big[(1-\beta)(\phi_s' + \mathrm{i}\kappa\,\psi_s) + \beta\,(\phi_f' + \mathrm{i}\kappa\,\psi_f)\big] - \phi' = 0\,,$$
$$(\mathrm{i}\kappa\,\phi_s - \psi_s')' + \mathrm{i}\kappa\,(\phi_s' + \mathrm{i}\kappa\,\psi_s) = 0\,,$$
$$-\mathrm{i}\,\omega\big[\lambda\,\nabla^2\phi_s + Q\,\nabla^2\phi_f + 2\mu_c\,(\phi_s' + \mathrm{i}\kappa\,\psi_s)'\big] + (1-\beta)\rho_s g\,\phi' - (1-\beta)\rho_f(-\omega^2\phi + g\,\phi') = 0\,,$$
$$-\mathrm{i}\,\omega\,(Q\,\nabla^2\phi_s + R\,\nabla^2\phi_f) + \beta\rho_f g\,\phi' - \beta\rho_f(-\omega^2\phi + g\,\phi') = 0\,,$$

- at the ocean floor $z = -H$

$$\phi' = 0.$$

Note that any constant term in conditions 1–8 may be eliminated by taking the time derivative of these equations. This amounts to multiplying the remaining terms by a common coefficient $-\mathrm{i}\,\omega$ which may then be factored and canceled out.

3. Dispersion relation

3.1. Derivation

Inserting the explicit expressions of the potentials in these boundary conditions leads to an algebraic homogeneous linear system of equations for constants C_i $(i = 1, \ldots, 8)$. Then demanding that the determinant of the associated 8×8 coefficient matrix be zero for nontrivial solutions yields the dispersion relation

$$\omega^2 = \left(\frac{T_1 + g\,T_2}{T_3}\right) D_4 \tanh(D_4 H)\,, \tag{29}$$

between κ and ω for gravity waves in a poroelastic ice layer. Note that the right-hand side of (29) also exhibits a dependence on ω. The coefficients T_1, T_2 and T_3 have lengthy expressions and thus are relegated to an appendix for the reader's convenience. Eq. (29) is derived with help from the software Mathematica.

For a given value of ω and other parameter values, this dispersion relation is solved numerically for κ using the root-finding routine *fsolve* in Matlab. More specifically, as κ is generally complex, Eq. (29) is split up into its real and imaginary parts. This leads to a system of two independent equations that are solved simultaneously for the two unknowns k and q. The *fsolve* algorithm is basically a quasi-Newton method with a numerical approximation of the Jacobian matrix. We have successfully used this Matlab routine in previous work [34,35] to compute solitary wave solutions of nonlinear partial differential equations. Since there are very likely multiple possible roots for k and q [28], we apply the selection criteria proposed in [6] to find a dominant pair (k, q) that would represent a physically relevant solution. Accordingly, we choose $(k, q) \in \mathbb{R}^2_+$ such that k is closest to the open-water wavenumber k_0 and q is the lowest attenuation rate possible. To do so, we run the root finder *fsolve* for a range of initial guesses around $k = k_0$ and $q = 0$, and select the converged values for which the error $|\kappa - (k_0 + \mathrm{i}\,0)|$ is minimum among all the solutions obtained. As pointed out in [26], alternate criteria for choosing κ may be needed but these are not explored in the present study. The WS procedure has the advantage of being relatively simple and was found to be sufficient for our purposes, producing nontrivial solutions of (29) in all the cases we examined and yielding satisfactory results for our poroelastic model in comparison with existing theories, as shown in the following tests.

Typical parameter values for sea ice that we specify in the computations are (in SI units, see Table 1): $g = 9.81$, $\rho_s = 917$, $\rho_f = 1025$, $c = 1449$, $\alpha = 5$, $\nu = 0.3$, $\mu = 2 \times 10^5$, and accordingly $K_s = 4.3 \times 10^5$, $K_f = K_s/4 = 1.1 \times 10^5$ [36,37]. We choose $H = 100$ m (relative to a representative ice thickness $h = 1$ m) to fall under deep-water conditions. Because of the large disparity in orders of magnitude among the various parameters, we find it convenient to non-dimensionalize the equations by using H as a characteristic length scale, $\sqrt{H/g}$ as a characteristic time scale and $\rho_f H^3$ as a characteristic mass. This non-dimensionalization contributes to the numerical well-conditioning of (29) and thus helps the root-finding process.

3.2. Limiting cases

Given the rather complicated nature of this poroelastic model and the large number of physical parameters, it is of interest to compare predictions from (29) with those from simpler existing models in their respective limits. This is accomplished by switching parameters off in (29). Because these existing models are for non-porous materials, we start with β and then switch more parameters off as the system is simplified.

3.2.1. Viscoelastic case

Setting $\beta = 0$, and allowing the bulk and shear moduli to be complex with imaginary parts, Eq. (29) reduces to a viscoelastic model for traveling waves in an ice layer. To compare with other such models [6,26], we define μ_c to be the complex Voigt shear modulus as given in (5). Eq. (29) then reads

$$\omega^2 = \left[g\left(1 - \frac{\rho_s}{\rho_f}\right) + \frac{T_4}{T_5}\right] D_4 \tanh(D_4 H)\,, \tag{30}$$

where

$$T_4 = g\rho_s D_9\big[D_7 \sinh(D_5 h) + D_8 \sinh(D_6 h)\big] + 2D_7 D_8\big[1 - \cosh(D_5 h)\cosh(D_6 h)\big] - (D_7^2 + D_8^2)\sinh(D_5 h)\sinh(D_6 h)\,,$$
$$T_5 = \rho_f D_9\big[D_7 \cosh(D_6 h)\sinh(D_5 h) + D_8 \cosh(D_5 h)\sinh(D_6 h)\big]\,,$$

and

$$D_5 = \sqrt{\kappa^2 - \frac{\rho_s\omega^2}{2\mu_c + \lambda}}\,,$$
$$D_6 = \sqrt{\kappa^2 - \frac{\rho_s\omega^2}{\mu_c}}\,,$$
$$D_7 = 4D_5 D_6 \kappa^2 \mu_c\,,$$
$$D_8 = (D_6^2 + \kappa^2)\big[\kappa^2\lambda - D_5^2(\lambda + 2\mu_c)\big]\,,$$
$$D_9 = D_5(D_6^2 - \kappa^2)\,.$$

Note that, as $h \to 0$ (shrinking ice thickness), $T_4/T_5 \to g\rho_s/\rho_f$ and Eq. (30) reduces to

$$\omega^2 = gD_4 \tanh(D_4 H)\,, \tag{31}$$

which is the dispersion relation for gravity waves on open water in the weakly compressible case.

As stated above, WS criteria are used to select κ as a function of ω among all the possible solutions of (30), with k_0 denoting hereafter the solution of (31). This open-water wavenumber is also determined numerically and was found to be similar to that in the incompressible case (1) for the range of ω being considered. In either case, the dispersion relation is relatively simple and can be easily solved, with only real roots k_0. Fig. 2 shows individual

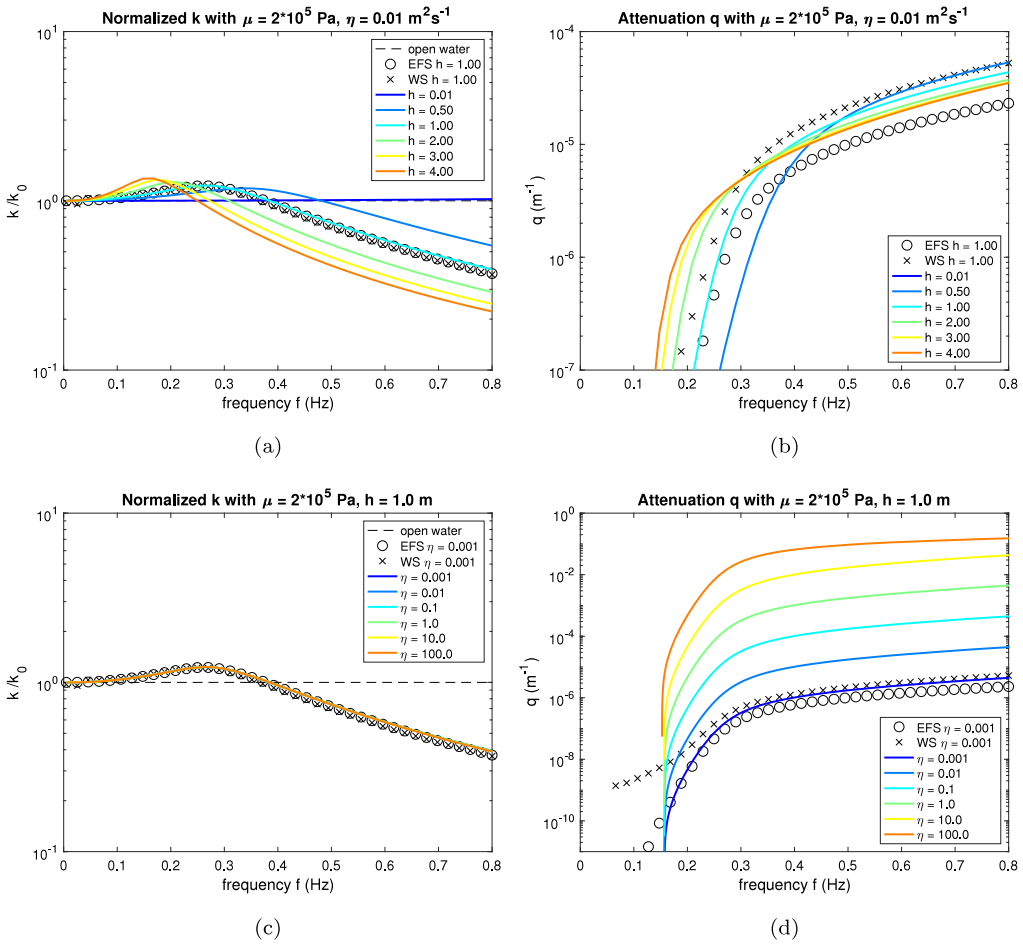

Fig. 2. Normalized wavenumber k/k_0 and attenuation rate q vs. frequency f for (a)–(b) varying ice thickness h and (c)–(d) varying viscosity η, in the non-porous viscoelastic case. Open-water, EFS and WS predictions are shown for comparison.

graphs of k and q as functions of frequency $f = 2\pi\omega$ for varying ice thickness h and viscosity η. As a reference, curves representing k_0 for open water and (k, q) from both EFS and WS models are also included in this figure. The same WS rule is applied to selecting solutions for these models. Although our computations were performed in terms of dimensionless quantities, our results are presented here in dimensional units to give the reader a better sense of actual physical scales.

Fig. 2(a)–(b) plot the normalized wavenumber k/k_0 and attenuation rate q versus frequency f for $\eta = 10^{-2}$ m^2 s^{-1} and $h = \{0.01, \ldots, 4.00\}$ m. We see that $k/k_0 < 1$ and decreases as f increases, except for a small range of frequencies near zero where this ratio is slightly larger than unity. Expectedly, $k/k_0 \to 1$ as $h \to 0$ (open-water limit). Our k-values compare well with EFS and WS predictions and, as an illustration (to avoid cluttering these figures), we only show the comparison for $h = 1$ m which is representative of first-year sea ice [26]. The q-curves on the other hand exhibit a more monotonic trend, continuously increasing with f. This increase is quite steep for low frequencies but is then much slower for higher frequencies. The larger h, the steeper this increase at low frequencies but the trend is reversed at higher frequencies where the larger h, the smaller the q-values. Although good agreement with WS predictions is again found for the entire range of frequencies considered, appreciable discrepancy with EFS results is observed at high frequencies. This may be expected considering that damping effects certainly depend strongly on h in the context of layer models while they likely do not for thin-plate models.

Recall that compressibility is allowed here, with both the floating ice layer and underlying ocean taken to be compressible media, while this is absent from the EFS and WS formulations. Therefore, given the same parameters h, μ and η, it is not surprising that small discrepancies are noticeable even in this non-porous viscoelastic case. Closer match is obtained between WS and our model because these describe two-layer systems while the EFS model is based on thin-plate theory. These small discrepancies tend to support the common assumption that compressional/stretching effects may be neglected for compact sea ice.

Fig. 2(c)–(d) depict k/k_0 and q versus f for $h = 1$ m and $\eta = \{10^{-3}, \ldots, 10^{2}\}$ m^2 s^{-1}. Overall, these graphs look similar to the previous ones. They suggest however that viscosity has no effect on k, only on q. The k-values seem to be insensitive to varying η and all fit onto a single curve. By contrast, the larger the viscosity, the stronger the attenuation at any frequency. The q-curves look alike but are shifted upward as η increases. Further comparison with the EFS and WS models is shown for $\eta = 10^{-3}$ m^2 s^{-1}, and the same observations as above can be made. Note that without the normalization by k_0, k would grow monotonically with f (see Fig. 3a), indicating a natural correspondence between wavelength (spatial scale) and wave period (temporal scale). Consequently, the fact that q also grows monotonically with f is consistent with the intuition that viscosity is stronger at smaller scales and thus shorter waves are more damped.

Similar results were reported by Collins et al. [25] in their review of existing models for wave propagation through sea ice.

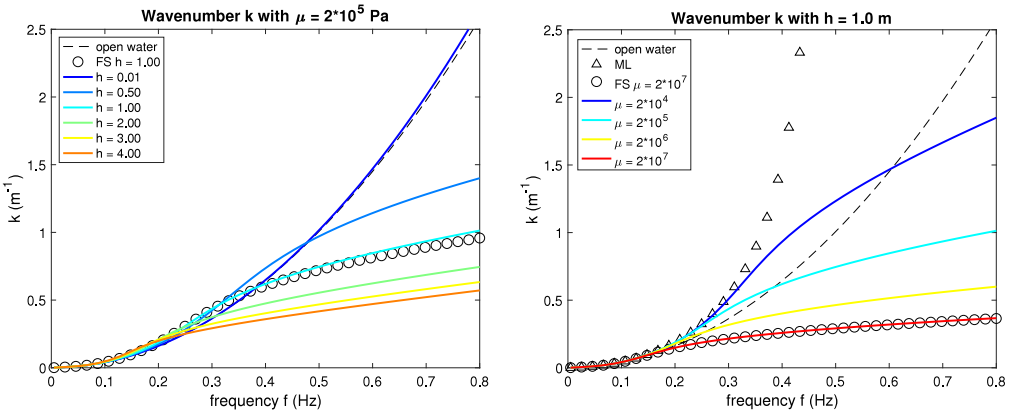

Fig. 3. Wavenumber k vs. frequency f for (a) varying ice thickness h and (b) varying shear modulus μ, in the non-porous elastic case. Open-water, FS and ML predictions are shown for comparison.

The slight increase of k/k_0 at low frequencies as shown in Fig. 2(a) and (c) is typical of mass loading, while the decrease at higher frequencies is attributed to elasticity. The slope change for q as observed in Fig. 2(b) and (d) also corresponds to the transition from mass loading to flexural rigidity as a dominant effect. Past this transition, the fact that short waves experience more attenuation in thinner ice (which is rather counter-intuitive) is reminiscent of a common feature in models for water waves over seabed composed of a viscous mud layer, where dissipation has a non-monotonic dependence on mud-layer thickness, with thicker layers being less dissipative [38].

3.2.2. Purely elastic case

In addition to $\beta = 0$, if viscosity is neglected (i.e. $\eta = 0$ and thus μ_c, K_c are real), then the constitutive laws for the ice layer simplify to those for an isotropic elastic material, as mentioned in Section 2.2.1. The resulting coupled system still views the underlying ocean as a weakly compressible fluid. In the absence of viscosity, for the infinite uniform domain depicted in Fig. 1, our continuum model only admits real roots of the dispersion relation. Its expression is pretty much identical to (30) with the exception that μ_c is replaced by μ. Fig. 3(a)–(b) show graphs of wavenumber k versus frequency f for varying ice thickness h (with $\mu = 2 \times 10^5$ Pa) and varying shear modulus μ (with $h = 1$ m). Shear modulus μ is a measure of the material rigidity, therefore higher μ is indicative of a stiffer ice cover.

We see that, in all cases, k grows monotonically with f. As $h \to 0$, these curves tend to a parabola over the entire range of frequencies considered, which is a characteristic shape for the dispersion relation in the open-water limit. In general however, two different trends can be discerned: a parabolic-like increase at low frequencies (which is slightly steeper than the open-water parabola) and a much slower increase at higher frequencies. The transition between these two trends appears as an inflection point on the curves and corresponds to the peak of k/k_0 as depicted in Fig. 2(a). Similar to the viscoelastic case, the former trend is a mass-loading effect as confirmed by the comparison with (2) in Fig. 3(b), while the latter trend is an elastic response that lessens k as μ increases. Therefore, at high frequencies, k is smaller than k_0, which is consistent with the fact that elasticity is a restoring force supplementing gravity in this problem and thus has a smoothing effect on wave motion [35,39,40]. Conversely, we observe that the mass-loading model is recovered as μ decreases. Our results are in excellent agreement with FS predictions for $kh \ll 1$, which is precisely the regime of validity for a thin elastic plate.

3.3. Porous case

We now examine the porous case by allowing $\beta \neq 0$ in (29). Recall that $\beta \in [0, 1]$ with $\beta = 0$ corresponding to a solid state (pack ice) and $\beta = 1$ corresponding to a fluid state (near-open water). As mentioned in Section 2.2.2, Biot's equations (16) and (17) for the ice layer can also describe friction due to the relative motion between the solid and fluid components, along with bulk viscous dissipation. This additional dissipative mechanism is represented by the parameter b, which depends on β as defined in (18). For the purposes of our analysis, we discuss the cases $b = 0$ and $b \neq 0$ separately, and in the former, we set $b = 0$ though $\beta \neq 0$. We first present results for $b = 0$ as this is a natural extension of the previous section and then turn our attention to the case $b \neq 0$. Because the present paper is focused on the development of our new model and its preliminary testing, we only show illustrative examples here and postpone a more detailed parametric study (including comparison with experimental data) to a future publication.

3.3.1. Porous elastic case

If μ_c and K_c are taken to be real (i.e. bulk viscosity is ignored), then the ice layer is viewed as a porous elastic material. With $b = 0$, all roots of (29) are real and we again follow WS criteria to select relevant solutions. Computations of k versus f are presented in Fig. 4 for $h = \{0.01, \ldots, 4.00\}$ m (with $\beta = 0.01$) and $\beta = \{0.01, \ldots, 0.99\}$ (with $h = 1$ m).

In Fig. 4(a), we check that results for $\beta = 0.01$ (very low porosity) are essentially identical to those for $\beta = 0$ as shown in Fig. 3(a). Expectedly, $k \to k_0$ as $h \to 0$ in this porous case too. Fig. 4(b) shows how the k-graph changes as β is varied over the range [0, 1]. Overall, k increases with β but the variations are rather mild and the dependence of k on f remains qualitatively the same as in the non-porous case, displaying two distinct behaviors at low and high frequencies as discussed earlier. Recall from Section 2.2.1 that the system retains strong elastic properties across the entire range of β, even at $\beta = 1$ where the solid and fluid constituents still coexist, and although K_f takes over K_s in this limit, these two parameters are comparable in magnitude. It is therefore not surprising that the graphs for varying β in Fig. 4(b) remain relatively close together. The limiting value $\beta = 1$ does not quite represent a pure fluid, even less an inviscid irrotational flow as assumed for the underlying ocean, and so k is not supposed to coincide with k_0. Nonetheless we see, especially at high frequencies, a tendency for k to move toward k_0 as $\beta \to 1$

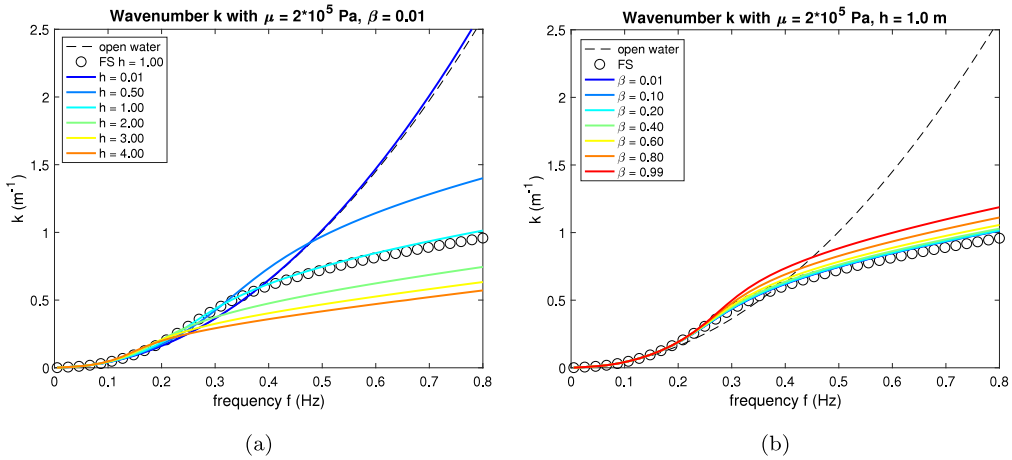

Fig. 4. Wavenumber k vs. frequency f for (a) varying ice thickness h and (b) varying porosity β, in the porous elastic case. Open-water and FS predictions are shown for comparison.

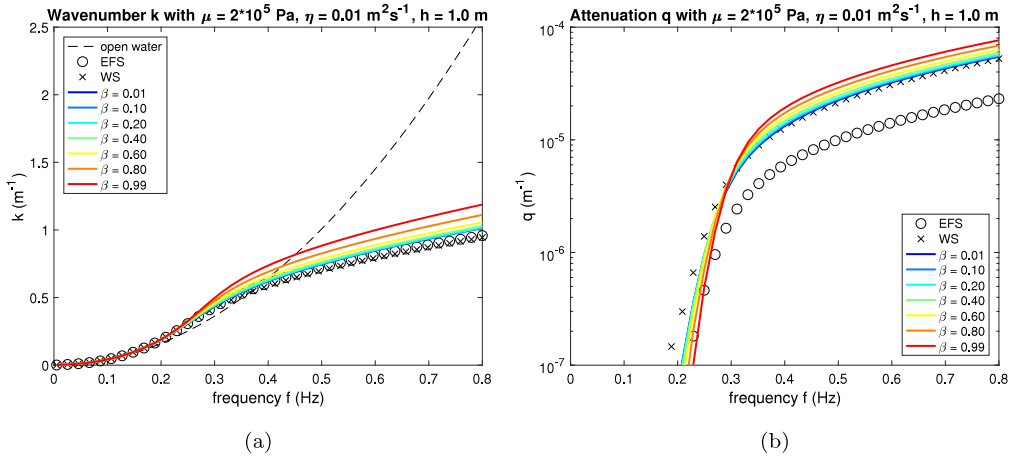

Fig. 5. (a) Wavenumber k and (b) attenuation rate q vs. frequency f for varying porosity β, in the porous viscoelastic case. Open-water, EFS and WS predictions are shown for comparison.

(fluid limit), and a good agreement with FS predictions as $\beta \to 0$ (solid limit).

3.3.2. Porous viscoelastic case

The porous model now incorporates bulk viscosity by allowing μ_c and K_c to be complex while keeping $b = 0$. Accordingly, the dispersion relation (29) also admits complex roots and, proceeding as in Section 3.2.1, we can determine κ given β and other physical parameters. Fig. 5 plots wavenumber k and attenuation rate q versus frequency f for $h = 1$ m, $\eta = 10^{-2}$ m^2 s^{-1} and varying β.

Fig. 5(a) for k bears resemblance to Fig. 4(b) in the porous elastic case, which confirms that viscosity has no influence on the wavenumber. Similar observations can be made about Fig. 5(b) for q. Little difference is seen as β is varied. The various q-graphs almost overlap and their general shape is identical to that illustrated in Fig. 2(b) for a non-porous viscoelastic ice layer. In general, the higher β, the larger k and q, and this behavior is more pronounced at higher frequencies. Close examination indicates that our results on k and q tend to converge to EFS and WS predictions as $\beta \to 0$, with a better agreement found on k. Our solutions for q compare well with WS predictions at low porosities, while EFS values remain visibly lower. All three models however display qualitatively the same properties of wave attenuation.

An exception may be made for WS q-curve whose drop as $f \to 0$ seems to slow down, in contrast to the EFS curve which quickly falls at low frequencies. This phenomenon is especially evident in Fig. 2(d) for a non-porous viscoelastic ice layer (see also Fig. 6b or d) and is consistent with results obtained in [25] for EFS and Keller's viscous-layer models. Interestingly, while our q-values are closer to WS predictions at higher frequencies, this trend is reversed at lower frequencies where our solutions behave more similarly to EFS predictions.

3.3.3. Porous frictional case

Our porous model is extended to the case $b \neq 0$, allowing for friction due to the relative motion between the solid and fluid constituents, along with viscous dissipation in the bulk of each phase. The roots of (29) are again complex and we anticipate this frictional mechanism would primarily affect the imaginary part of κ corresponding to the attenuation rate q. The coefficient of permeability K_p in the definition (18) of b may be estimated by

$$K_p = \frac{\beta a^2}{8}, \tag{32}$$

where a is a measure of the pore size, as proposed in [20,36]. Understandably, permeability (i.e. the ability of a porous material to allow fluids to pass through it) depends on porosity and pore size. That b is inversely proportional to K_p reflects the fact that the more permeable the medium, the larger the difference

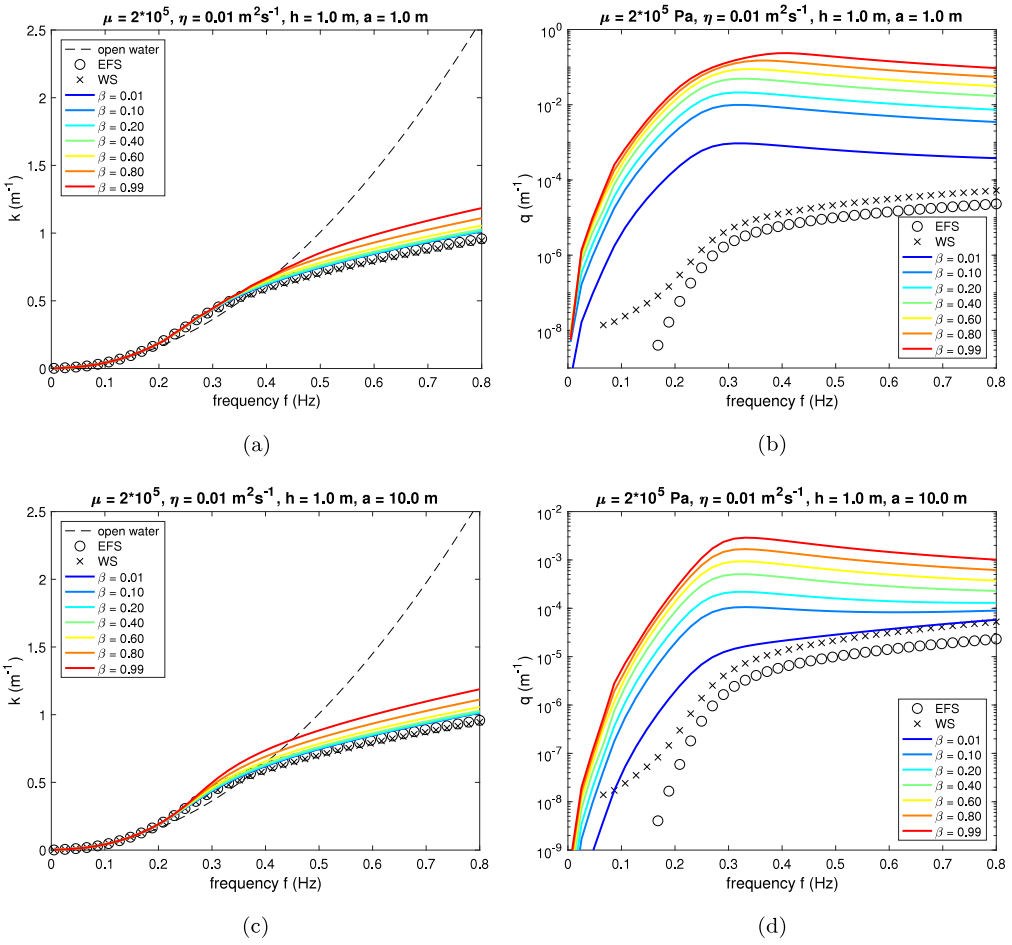

Fig. 6. Wavenumber k and attenuation rate q vs. frequency f for varying porosity β, in the porous frictional case with (a)–(b) $a = 1$ m and (c)–(d) $a = 10$ m. Open-water, EFS and WS predictions are shown for comparison.

between solid and fluid motions, hence the stronger the friction. Combining (18) and (32) reveals that b depends linearly on β, and thus friction is directly connected to the porous nature of the ice cover. Because b is proportional to η as well, if $\eta = 0$, then the porous elastic case (without viscosity or friction) is recovered.

Fig. 6 depicts k and q versus f for $h = 1$ m, $\eta = 10^{-2}$ m^2 s^{-1}, $a = \{1, 10\}$ m and varying β. Bear in mind that fluid pores may here represent areas of open water across the ice field. As expected, the k-graphs closely resemble those in Fig. 5(a) for a porous viscoelastic ice layer. This result confirms that the wavenumber is insensitive to any dissipative effect in the present model. However, unlike Fig. 5(b), the attenuation rate now exhibits much stronger dependence on porosity. We observe again that q increases with β, which is not surprising since b (and hence friction) strengthens as β increases, but this rise in q is quite significant for the range of $\beta \in [0, 1]$, spanning several orders of magnitude above EFS and WS values (which serve as a reference for the non-porous frictionless limit as $\beta \to 0$). For a given η (bulk viscosity), the attenuation rate is thus amplified in the presence of friction ($b \neq 0$). Because of the direct relationship between a, b and β through (18) and (32), we would obtain plots similar to Fig. 6 by varying a or K_p while fixing β.

Another striking difference compared to Fig. 5(b) for varying β or Fig. 2(d) for varying η is that the dependence of q on f is no longer monotonic: q quickly grows to a maximum around $f = 0.3$ Hz before slowly decaying at higher frequencies. This maximum seems to coincide with the transition point from mass loading to flexural rigidity as discussed in Section 3.2.1. Interestingly, Fig. 6(b) and (d) are reminiscent of the roll-over phenomenon that has been reported in field observations [7,17]. Here, the higher the porosity, the more pronounced this roll-over in attenuation plots. Continuum (visco)elastic models or discrete scattering models have usually been unable to predict this phenomenon [2,6]. Possible explanations that have been suggested include wind forcing and nonlinear wave interactions [13,41]. Although it is difficult to discriminate one particular mechanism in the present continuum setting, our linear results indicate that the relative motions between different constituents of the ice cover (e.g. ice floes, pancake ice, brash ice) induce friction that may interfere with other dissipative effects to help produce the non-monotonic (roll-over) behavior of q as a function of f, which has been observed in the MIZ. Given the possible large repercussions associated with friction as illustrated in Fig. 6, this dissipative mechanism may play an important role in applications of our poroelastic model to wave-ice interactions.

3.3.4. Porous asymptotic case

Because the porosity is by definition a small dimensionless parameter ($0 \leq \beta \leq 1$), it is natural to seek an alternate expression for the dispersion relation (29) with a more explicit dependence on β. This can be accomplished by exploiting the exact character of (29) and by Taylor expanding it, say, up to first order in β. In this process, all parameters that depend on β are expanded, including e.g. Lamé's parameter

$$\lambda = \lambda^{(0)} + \lambda^{(1)}\beta,$$

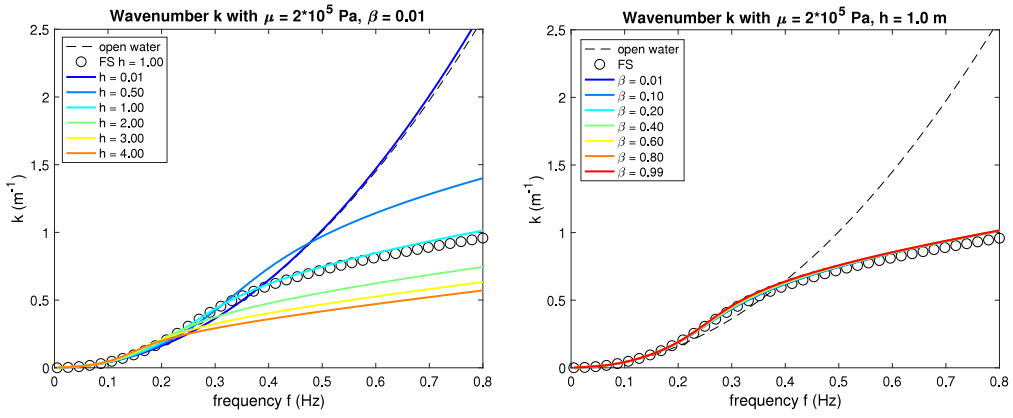

Fig. 7. Wavenumber k vs. frequency f for (a) varying ice thickness h and (b) varying porosity β, in the porous asymptotic case ($\eta = 0$). Open-water and FS predictions are shown for comparison.

where

$$\lambda^{(0)} = K_s - \frac{2}{3}\mu_c\,,$$

$$\lambda^{(1)} = -K_s n + \frac{K_f K_s(-1+n)^2}{K_s + K_f(-1+n)}\,.$$

Putting all the contributions together, the Taylor expansion of (29) up to first order in β can be written as

$$\omega^2 = (T_0^{(0)} + T_0^{(1)}\beta)D_4^{(0)}\tanh(D_4^{(0)}H)\,, \tag{33}$$

where

$$T_0^{(0)} = \frac{T_1^{(0)} + g\,T_2^{(0)}}{T_3^{(0)}}\,,$$

$$T_0^{(1)} = \frac{T_3^{(0)}T_1^{(1)} - T_3^{(1)}T_1^{(0)} + g\,T_3^{(0)}T_2^{(1)} - g\,T_3^{(1)}T_2^{(0)}}{{T_3^{(0)}}^2}\,.$$

We emphasize that, in this asymptotic form, the coefficients $T_0^{(0)}$, $T_0^{(1)}$ and $D_4^{(0)}$ are not functions of β though they still exhibit a dependence on ω. Their lengthy expressions together with expansions of Biot's parameters are relegated to an appendix for the reader's convenience. Because ice concentration is an important factor in characterizing and modeling the sea-ice cover, Eq. (33) with such a simple dependence on β may be helpful in estimating ice concentration from the knowledge of other ice and wave parameters. This inverse problem is outside the scope of the present paper and is envisioned for future work.

Unfortunately, our perturbation calculations suggest that Eq. (33) only applies to the porous elastic case ($\eta = 0$). For a porous viscoelastic layer ($\eta \neq 0$) with complex shear modulus given by (5), first-order terms in β seem to cancel out and the next-order nonzero contributions are of second order. These however produce lengthier expressions and thus make the asymptotic approximation less appealing in this case. Taking μ_c and K_c to be real, computations of k versus f based on (33) are shown in Fig. 7(a) for $\beta = 0.01$ and varying h, and in Fig. 7(b) for $h = 1$ m and varying β. As expected, these results are similar to those obtained in the porous elastic limit (see Fig. 4) with the full dispersion relation (29). A noticeable difference between Fig. 4(b) and 7(b) is that the k-graphs for varying β remain very close together in the asymptotic case, which is indicative that (33) may not be suitable over the entire range $\beta \in [0, 1]$. This result is not too surprising given the fact that a first-order approximation such as (33) would be accurate only for very small β, which may be viewed as a limitation for the aforementioned inverse problem. Further investigation is needed in this regard and is left for future work, possibly examining both (29) and (33).

4. Conclusions

We have proposed a two-dimensional continuum model for linear wave propagation across ice-infested seas. It is based on a two-layer formulation where the floating sea ice is described as a homogeneous isotropic poroelastic material according to Biot's theory, and the underlying ocean is viewed as a weakly compressible fluid. Dissipative effects are included in this formulation via two distinct mechanisms: viscosity in the bulk of the ice layer, and friction caused by the relative motion between its solid and fluid constituents. In view are potential applications to modeling wave scattering and attenuation in the MIZ. A parameter of special interest in our wave-ice model is the porosity, whose complement may serve as a measure of ice concentration in the ice field.

We have established an exact dispersion relation for surface traveling waves in this coupled system and obtained numerical estimates of its complex roots. For a given frequency, the real and imaginary parts of these roots represent the wavenumber and attenuation rate in the horizontal direction, respectively. Despite the complicated nature of this dispersion relation, we were able to find relevant solutions in all the cases we considered, using a well-established root-finding method together with relatively simple selection criteria.

We have conducted extensive tests to examine the dependence of solutions on various parameters in both the porous and non-porous cases, and performed detailed comparisons with other models. Given the good agreement found overall, these results help validate our new poroelastic formulation against existing elastic and viscoelastic models in their respective limits, and in turn also help validate these simpler models against a more general representation of the ice-ocean system. Overall, both the wavenumber and attenuation rate are found to be increasing functions of frequency, although their slopes are not monotonic functions because they are indicative of the relative importance of various rheological effects (e.g. mass loading, elasticity) as frequency is varied.

A more complex picture arises when friction is taken into account, showing a non-monotonic behavior of attenuation rate as a function of frequency, which is reminiscent of the roll-over phenomenon that has been reported in field observations. This finding highlights the role of porosity in the present description of wave-ice interactions, as friction is directly connected

to the porous nature of the ice cover. Significant quantitative and qualitative differences in wave attenuation are observed as compared to the frictionless case. It is suggested that friction may interfere with bulk viscosity to produce the observed non-monotonic behavior. This dissipative mechanism could possibly be a contributing factor in the roll-over phenomenon arising from field observations.

Finally, we have also derived an alternate form of the dispersion relation, which displays a more explicit dependence on porosity. This is accomplished via a first-order Taylor expansion by exploiting the smallness of the corresponding parameter. It is anticipated that such an approximation of the dispersion relation may be helpful in obtaining information on ice concentration from the knowledge of other ice and wave parameters.

A natural next step would be to provide a detailed assessment of our model predictions against experimental data [7,15,42,43]. Considering the large parameter space associated with our poroelastic formulation as well as the possible need for more refined criteria in the search of relevant solutions, this investigation is envisioned for future work. It would also be of interest to examine nonlinear extensions of our poroelastic model. Nonlinear theory of wave-ice interactions has received increasing attention in recent years [35,39,40,44,45].

Acknowledgments

This work is partially supported by the National Science Foundation, USAthrough grant number DMS-1615480. P. Guyenne also thanks the Tsinghua Sanya International Mathematics Forum (China) for its hospitality during a visit in the winter 2019.

Appendix. Coefficients in the dispersion relation

A.1. General case

Coefficients in the full dispersion relation (29) have the following expressions:

$$
\begin{aligned}
T_1 =\ & 2E_1E_{12}[E_2E_{23}(1-\cosh(D_1h)\cosh(D_3h))\sinh(D_2h)\\
& -E_1E_{13}(1-\cosh(D_1h)\cosh(D_2h))\sinh(D_3h)]\\
& +\sinh(D_1h)[2E_1E_{13}E_2E_{23}(-1+\cosh(D_2h)\cosh(D_3h))\\
& -(E_1^2(E_{12}^2+E_{13}^2)+E_2^2E_{23}^2)\sinh(D_2h)\sinh(D_3h)]\ ,\\
T_2 =\ & E_1[(E_{17}E_4E_7+E_{18}E_6E_9)(1-\cosh(D_1h)\cosh(D_2h))\\
& -(E_{14}E_2E_{21}E_7-E_{20}E_5E_9)(1-\cosh(D_1h)\cosh(D_3h))\\
& -(E_{19}E_4E_5-E_{14}E_2E_{22}E_6)(1-\cosh(D_2h)\cosh(D_3h))]\\
& -E_1[(E_{17}E_3E_7+E_{18}E_6E_8)(1-\cosh(D_1h)\\
& \times\cosh(D_2h))\cosh(D_3h)\\
& +(E_{16}E_2E_{21}E_7-E_{20}E_5E_8)\cosh(D_2h)\\
& \times(-1+\cosh(D_1h)\cosh(D_3h))\\
& +(E_{19}E_3E_5-E_{16}E_2E_{22}E_6)\cosh(D_1h)\\
& \times(-1+\cosh(D_2h)\cosh(D_3h))]\\
& +E_1(E_{12}E_4E_6+E_{13}E_7E_9)\sinh(D_1h)\sinh(D_2h)\\
& -E_1(E_{12}E_3E_6+E_{13}E_7E_8)\cosh(D_3h)\sinh(D_1h)\sinh(D_2h)\\
& +(E_1^2E_{12}E_{14}E_5-E_2E_{23}E_7E_9)\sinh(D_1h)\sinh(D_3h)\\
& -(E_1^2E_{12}E_{16}E_5-E_2E_{23}E_7E_8)\cosh(D_2h)\sinh(D_1h)\sinh(D_3h)\\
& -(E_1^2E_{13}E_{14}E_5-E_2E_{23}E_4E_6)\sinh(D_2h)\sinh(D_3h)\\
& +(E_1^2E_{13}E_{16}E_5-E_2E_{23}E_3E_6)\cosh(D_1h)\sinh(D_2h)\sinh(D_3h)\ ,\\
T_3 =\ & E_1[(E_{11}E_{18}E_6+E_{10}E_{17}E_7)\\
& \times(1-\cosh(D_1h)\cosh(D_2h))\cosh(D_3h)\\
& -(E_{11}E_{20}E_5-E_{15}E_2E_{21}E_7)\cosh(D_2h)\\
& \times(-1+\cosh(D_1h)\cosh(D_3h))\\
& +(E_{10}E_{19}E_5-E_{15}E_2E_{22}E_6)\cosh(D_1h)\\
& \times(-1+\cosh(D_2h)\cosh(D_3h))]\\
& +E_1(E_{10}E_{12}E_6+E_{11}E_{13}E_7)\cosh(D_3h)\sinh(D_1h)\sinh(D_2h)\\
& +(E_1^2E_{12}E_{15}E_5-E_{11}E_2E_{23}E_7)\cosh(D_2h)\sinh(D_1h)\sinh(D_3h)\\
& -(E_1^2E_{13}E_{15}E_5-E_{10}E_2E_{23}E_6)\cosh(D_1h)\sinh(D_2h)\sinh(D_3h)\ ,
\end{aligned}
$$

and the $E_i\,(i=1,\dots,23)$ are defined as follows:

$$
\begin{aligned}
E_1 &= 2D_3\kappa^2\mu_c\ ,\\
E_2 &= -(D_2^2-\kappa^2)(F_6Q+F_8R)(-\kappa^2(F_7Q+F_5\lambda)\\
&\quad +D_1^2(F_7Q+F_5(\lambda+2\mu_c)))\\
&\quad +(D_1^2-\kappa^2)(F_5Q+F_7R)(-\kappa^2(F_8Q+F_6\lambda)\\
&\quad +D_2^2(F_8Q+F_6(\lambda+2\mu_c)))\ ,\\
E_3 &= -(D_2^2-\kappa^2)(F_6Q+F_8R)(\rho_s-\rho_f)(1-\beta)\ ,\\
E_4 &= -(D_2^2-\kappa^2)(F_6Q+F_8R)\rho_s(1-\beta)\\
&\quad +\rho_w\beta[-\kappa^2(F_8Q+F_6\lambda)+D_2^2(F_8Q+F_6(\lambda+2\mu_c))]\ ,\\
E_5 &= -2D_1D_2F_6(F_5(-1+\beta)-F_7\beta)\\
&\quad +2D_1D_2F_5(F_6(-1+\beta)-F_8\beta)\ ,\\
E_6 &= D_1(D_3^2+\kappa^2)(F_5(-1+\beta)-F_7\beta)\\
&\quad +2D_1F_5\kappa^2(1+(-1+F9)\beta)\ ,\\
E_7 &= D_2(D_3^2+\kappa^2)(F_6(-1+\beta)-F_8\beta)\\
&\quad +2D_2F_6\kappa^2(1+(-1+F9)\beta)\ ,\\
E_8 &= -(D_1^2-\kappa^2)(F_5Q+F_7R)(\rho_s-\rho_f)(1-\beta)\ ,\\
E_9 &= -(D_1^2-\kappa^2)(F_5Q+F_7R)\rho_s(1-\beta)\\
&\quad +\rho_f\beta[-\kappa^2(F_7Q+F_5\lambda)+D_1^2(F_7Q+F_5(\lambda+2\mu_c))]\ ,\\
E_{10} &= -(D_2^2-\kappa^2)(F_6Q+F_8R)\rho_f(1-\beta)\\
&\quad +\rho_f\beta[-\kappa^2(F_8Q+F_6\lambda)+D_2^2(F_8Q+F_6(\lambda+2\mu_c))]\ ,\\
E_{11} &= -(D_1^2-\kappa^2)(F_5Q+F_7R)\rho_f(1-\beta)\\
&\quad +\rho_f\beta[-\kappa^2(F_7Q+F_5\lambda)+D_1^2(F_7Q+F_5(\lambda+2\mu_c))]\ ,\\
E_{12} &= 2D_1F_5(D_2^2-\kappa^2)(F_6Q+F_8R)\ ,\\
E_{13} &= 2D_2F_6(D_1^2-\kappa^2)(F_5Q+F_7R)\ ,\\
E_{14} &= \rho_f\beta\ ,\\
E_{15} &= \rho_f\beta\ ,\\
E_{16} &= 0\ ,\\
E_{17} &= 2D_1F_5(D_1^2-\kappa^2)(F_5Q+F_7R)\ ,\\
E_{18} &= 2D_2F_6(D_2^2-\kappa^2)(F_6Q+F_8R)\ ,\\
E_{19} &= (D_1^2-\kappa^2)(D_3^2+\kappa^2)(F_5Q+F_7R)\ ,\\
E_{20} &= (D_2^2-\kappa^2)(D_3^2+\kappa^2)(F_6Q+F_8R)\ ,\\
E_{21} &= 2D_1F_5\ ,\\
E_{22} &= 2D_2F_6\ ,\\
E_{23} &= D_3^2+\kappa^2\ .
\end{aligned}
$$

A.2. Asymptotic case

Coefficients in the truncated dispersion relation (33) have the following expressions:

$$
\lambda^{(0)}=K_s-\frac{2\mu}{3}\ ,\quad \lambda^{(1)}=-K_sn+\frac{K_fK_s(-1+n)^2}{K_s+K_f(-1+n)}\ ,
$$

$$
Q^{(1)}=\frac{K_fK_s(-1+n)}{K_s+K_f(-1+n)}\ ,\quad R^{(1)}=\frac{K_fK_s}{K_s+K_f(-1+n)}\ ,
$$

$$r_{11}^{(0)} = \rho_s\ , \quad r_{11}^{(1)} = -\rho_s - \rho_f(1-\alpha)\ , \quad r_{12}^{(1)} = \rho_f(1-\alpha)\ ,$$
$$r_{22}^{(1)} = \rho_f\alpha\ ,$$
$$a_{11}^{(0)} = \frac{1}{\lambda^{(0)}+2\mu}\ , \quad a_{11}^{(1)} = \frac{Q^{(1)^2} - R^{(1)}\lambda^{(1)}}{R^{(1)}(\lambda^{(0)}+2\mu)^2}\ ,$$
$$a_{12}^{(0)} = \frac{Q^{(1)}}{R^{(1)}(\lambda^{(0)}+2\mu)}\ , \quad a_{12}^{(1)} = \frac{Q^{(1)}(Q^{(1)^2} - R^{(1)}\lambda^{(1)})}{R^{(1)^2}(\lambda^{(0)}+2\mu)^2}\ ,$$
$$a_{22}^{(-1)} = \frac{1}{R^{(1)}}\ , \quad a_{22}^{(0)} = \frac{Q^{(1)^2}}{R^{(1)^2}(\lambda^{(0)}+2\mu)}\ ,$$
$$a_{22}^{(1)} = \frac{Q^{(1)^2}(Q^{(1)^2} - R^{(1)}\lambda^{(1)})}{(R^{(1)})^3(\lambda^{(0)}+2\mu)^2}\ ,$$
$$B_{11}^{(0)} = a_{11}^{(0)}r_{11}^{(0)}\omega^2\ , \quad B_{11}^{(1)} = (a_{11}^{(0)}r_{11}^{(1)} + a_{11}^{(1)}r_{11}^{(0)} - a_{12}^{(0)}r_{12}^{(1)})\omega^2\ ,$$
$$B_{12}^{(0)} = (-a_{12}^{(0)}r_{11}^{(0)} + a_{22}^{(-1)}r_{12}^{(1)})\omega^2\ ,$$
$$B_{12}^{(1)} = -(a_{12}^{(0)}r_{11}^{(1)} + a_{12}^{(1)}r_{11}^{(0)} - a_{22}^{(0)}r_{12}^{(1)})\omega^2\ ,$$
$$B_{21}^{(1)} = (a_{11}^{(0)}r_{12}^{(1)} - a_{12}^{(0)}r_{22}^{(1)})\omega^2\ ,$$
$$B_{22}^{(0)} = a_{22}^{(-1)}r_{22}^{(1)}\omega^2\ , \quad B_{22}^{(1)} = (-a_{12}^{(0)}r_{12}^{(1)} + a_{22}^{(0)}r_{22}^{(1)})\omega^2\ ,$$
$$D_1^{(0)} = \sqrt{\frac{-F_1^{(0)} - \sqrt{F_1^{(0)^2} - 4F_2^{(0)}}}{2}}\ ,$$
$$D_1^{(1)} = \frac{2F_2^{(1)} - F_1^{(1)}(F_1^{(0)} + \sqrt{F_1^{(0)^2} - 4F_2^{(0)}})}{2\sqrt{2}\sqrt{-F_1^{(0)} - \sqrt{F_1^{(0)^2} - 4F_2^{(0)}}}\sqrt{F_1^{(0)^2} - 4F_2^{(0)}}}\ ,$$
$$D_2^{(0)} = \sqrt{\frac{-F_1^{(0)} + \sqrt{F_1^{(0)^2} - 4F_2^{(0)}}}{2}}\ ,$$
$$D_2^{(1)} = -\frac{2F_2^{(1)} + F_1^{(1)}(-F_1^{(0)} + \sqrt{F_1^{(0)^2} - 4F_2^{(0)}})}{2\sqrt{2}\sqrt{-F_1^{(0)} + \sqrt{F_1^{(0)^2} - 4F_2^{(0)}}}\sqrt{F_1^{(0)^2} - 4F_2^{(0)}}}\ ,$$
$$D_3^{(0)} = \sqrt{k^2 - \frac{r_{11}^{(0)}\omega^2}{\mu}}\ , \quad D_3^{(1)} = \frac{(\rho_f(-1+\alpha)^2 - r_{11}^{(1)}\alpha)\omega^2}{2\alpha\mu D_3^{(0)}}\ ,$$
$$D_4^{(0)} = \sqrt{k^2 - \frac{\omega^2}{c^2}}\ ,$$

$$F_1^{(0)} = B_{11}^{(0)} + B_{22}^{(0)} - 2k^2\ , \quad F_1^{(1)} = (B_{11}^{(1)} + B_{22}^{(1)})\ ,$$
$$F_2^{(0)} = (B_{11}^{(0)} - k^2)(B_{22}^{(0)} - k^2)\ ,$$
$$F_2^{(1)} = -B_{12}^{(0)}B_{21}^{(1)} + B_{11}^{(0)}B_{22}^{(1)} + B_{11}^{(1)}B_{22}^{(0)} - (B_{11}^{(1)} + B_{22}^{(1)})k^2\ ,$$
$$F_3^{(0)} = -\frac{B_{11}^{(0)} + D_1^{(0)^2} - k^2}{B_{12}^{(0)}}\ , \quad F_4^{(0)} = -\frac{B_{11}^{(0)} + D_2^{(0)^2} - k^2}{B_{12}^{(0)}}\ ,$$
$$F_3^{(1)} = \frac{-B_{12}^{(0)}(B_{11}^{(1)} + 2D_1^{(1)}D_1^{(0)}) + B_{12}^{(1)}(B_{11}^{(0)} + D_1^{(0)^2} - k^2)}{B_{12}^{(0)^2}}\ ,$$
$$F_4^{(1)} = \frac{-B_{12}^{(0)}(B_{11}^{(1)} + 2D_2^{(1)}D_2^{(0)}) + B_{12}^{(1)}(B_{11}^{(0)} + D_2^{(0)^2} - k^2)}{B_{12}^{(0)^2}}\ ,$$
$$F_5^{(0)} = a_{11}^{(0)} - a_{12}^{(0)}F_3^{(0)}\ , \quad F_5^{(1)} = (a_{11}^{(1)} - a_{12}^{(0)}F_3^{(1)} - a_{12}^{(1)}F_3^{(0)})\ ,$$
$$F_6^{(0)} = a_{11}^{(0)} - a_{12}^{(0)}F_4^{(0)}\ , \quad F_6^{(1)} = (a_{11}^{(1)} - a_{12}^{(0)}F_4^{(1)} - a_{12}^{(1)}F_4^{(0)})\ ,$$
$$F_7^{(-1)} = a_{22}^{(-1)}F_3^{(0)}\ , \quad F_8^{(-1)} = a_{22}^{(-1)}F_4^{(0)}\ , \quad F_9^{(0)} = -\frac{1-\alpha}{\alpha}\ ,$$
$$F_7^{(0)} = -a_{12}^{(0)} + a_{22}^{(-1)}F_3^{(1)} + a_{22}^{(0)}F_3^{(0)}\ ,$$
$$F_7^{(1)} = (-a_{12}^{(1)} + a_{22}^{(0)}F_3^{(1)} + a_{22}^{(1)}F_3^{(0)})\ ,$$
$$F_8^{(0)} = -a_{12}^{(0)} + a_{22}^{(-1)}F_4^{(1)} + a_{22}^{(0)}F_4^{(0)}\ ,$$
$$F_8^{(1)} = (-a_{12}^{(1)} + a_{22}^{(0)}F_4^{(1)} + a_{22}^{(1)}F_4^{(0)})\ ,$$
$$E_1^{(0)} = 2D_3^{(0)}k^2\mu\ , \quad E_1^{(1)} = 2D_3^{(1)}k^2\mu\ ,$$
$$\begin{aligned}E_2^{(0)} = {} & k^2R^{(1)}((F_6^{(0)}F_7^{(-1)} - F_5^{(0)}F_8^{(-1)})k^2\lambda^{(0)} + D_2^{(0)^2}(F_5^{(0)}F_8^{(-1)}\lambda^{(0)} \\ & - F_6^{(0)}F_7^{(-1)}(\lambda^{(0)}+2\mu))) \\ & + D_1^{(0)^2}R^{(1)}(D_2^{(0)^2}(F_6^{(0)}F_7^{(-1)} - F_5^{(0)}F_8^{(-1)})(\lambda^{(0)} \\ & + 2\mu) + k^2(-F_6^{(0)}F_7^{(-1)}\lambda^{(0)} + F_5^{(0)}F_8^{(-1)}(\lambda^{(0)}+2\mu)))\ ,\end{aligned}$$
$$\begin{aligned}E_2^{(1)} = {} & F_8^{(-1)}(-D_2^{(0)^2} + k^2)R^{(1)}(-k^2(F_7^{(0)}Q^{(1)} + F_5^{(0)}\lambda^{(1)} + F_5^{(1)}\lambda^{(0)}) \\ & + D_1^{(0)^2}(F_7^{(0)}Q^{(1)} + F_5^{(0)}\lambda^{(1)} + F_5^{(1)}\lambda^{(0)} \\ & + 2F_5^{(1)}\mu) + 2D_1^{(1)}D_1^{(0)}(F_7^{(-1)}Q^{(1)} \\ & + F_5^{(0)}(\lambda^{(0)}+2\mu))) + (-2D_2^{(1)}D_2^{(0)}F_8^{(-1)}R^{(1)} \\ & + (-D_2^{(0)^2} + k^2)(F_6^{(0)}Q^{(1)} \\ & + F_8^{(0)}R^{(1)}))(-k^2(F_7^{(-1)}Q^{(1)} + F_5^{(0)}\lambda^{(0)}) \\ & + D_1^{(0)^2}(F_7^{(-1)}Q^{(1)} + F_5^{(0)}(\lambda^{(0)}+2\mu))) \\ & + F_7^{(-1)}(D_1^{(0)^2} - k^2)R^{(1)}(-k^2(F_8^{(0)}Q^{(1)} + F_6^{(0)}\lambda^{(1)} + F_6^{(1)}\lambda^{(0)}) \\ & + D_2^{(0)^2}(F_8^{(0)}Q^{(1)} \\ & + F_6^{(0)}\lambda^{(1)} + F_6^{(1)}\lambda^{(0)} + 2F_6^{(1)}\mu) + 2D_2^{(1)}D_2^{(0)}(F_8^{(-1)}Q^{(1)} \\ & + F_6^{(0)}(\lambda^{(0)}+2\mu))) \\ & + (2D_1^{(1)}D_1^{(0)}F_7^{(-1)}R^{(1)} + (D_1^{(0)^2} - k^2)(F_5^{(0)}Q^{(1)} \\ & + F_7^{(0)}R^{(1)}))(-k^2(F_8^{(-1)}Q^{(1)} \\ & + F_6^{(0)}\lambda^{(0)}) + D_2^{(0)^2}(F_8^{(-1)}Q^{(1)} + F_6^{(0)}(\lambda^{(0)}+2\mu)))\ ,\end{aligned}$$
$$E_3^{(0)} = F_8^{(-1)}(-D_2^{(0)^2} + k^2)R^{(1)}(\rho_s - \rho_f)\ ,$$
$$\begin{aligned}E_3^{(1)} = {} & (\rho_s - \rho_f)(F_8^{(-1)}(-2D_2^{(1)}D_2^{(0)} + D_2^{(0)^2} - k^2)R^{(1)} \\ & + (-D_2^{(0)^2} + k^2)(F_6^{(0)}Q^{(1)} + F_8^{(0)}R^{(1)}))\ ,\end{aligned}$$
$$E_4^{(0)} = F_8^{(-1)}(-D_2^{(0)^2} + k^2)R^{(1)}\rho_s\ ,$$
$$\begin{aligned}E_4^{(1)} = {} & -2D_2^{(1)}D_2^{(0)}F_8^{(-1)}R^{(1)}\rho_s + k^2(F_8^{(0)}R^{(1)}\rho_s \\ & - F_8^{(-1)}(R^{(1)}\rho_s + Q^{(1)}\rho_f) \\ & + F_6^{(0)}(Q^{(1)}\rho_s - \rho_f\lambda^{(0)})) + D_2^{(0)^2}(-F_6^{(0)}Q^{(1)}\rho_s \\ & + F_8^{(-1)}R^{(1)}\rho_s - F_8^{(0)}R^{(1)}\rho_s \\ & + F_8^{(-1)}Q^{(1)}\rho_f + F_6^{(0)}\rho_f(\lambda^{(0)}+2\mu))\ ,\end{aligned}$$
$$E_5^{(0)} = 2D_1^{(0)}D_2^{(0)}(F_6^{(0)}F_7^{(-1)} - F_5^{(0)}F_8^{(-1)})\ ,$$
$$\begin{aligned}E_5^{(1)} = {} & 2(D_1^{(1)}D_2^{(0)}(F_6^{(0)}F_7^{(-1)} - F_5^{(0)}F_8^{(-1)}) \\ & + D_1^{(0)}(D_2^{(1)}(F_6^{(0)}F_7^{(-1)} - F_5^{(0)}F_8^{(-1)}) \\ & + D_2^{(0)}(F_6^{(1)}F_7^{(-1)} + F_6^{(0)}F_7^{(0)} - F_5^{(1)}F_8^{(-1)} - F_5^{(0)}F_8^{(0)})))\ ,\end{aligned}$$
$$E_6^{(0)} = 2D_1^{(0)}F_5^{(0)}k^2 - D_1^{(0)}(F_5^{(0)} + F_7^{(-1)})(D_3^{(0)^2} + k^2)\ ,$$
$$\begin{aligned}E_6^{(1)} = {} & 2(D_1^{(1)}F_5^{(0)} + D_1^{(0)}(F_5^{(1)} + F_5^{(0)}(-1 + F_9^{(0)})))k^2 - D_1^{(0)}(F_5^{(1)} - F_5^{(0)} \\ & + F_7^{(0)})(D_3^{(0)^2} + k^2) - (F_5^{(0)} + F_7^{(-1)})(2D_1^{(0)}D_3^{(1)}D_3^{(0)} \\ & + D_1^{(1)}(D_3^{(0)^2} + k^2))\ ,\end{aligned}$$
$$E_7^{(0)} = 2D_2^{(0)}F_6^{(0)}k^2 - D_2^{(0)}(F_6^{(0)} + F_8^{(-1)})(D_3^{(0)^2} + k^2)\ ,$$
$$\begin{aligned}E_7^{(1)} = {} & 2(D_2^{(1)}F_6^{(0)} + D_2^{(0)}(F_6^{(1)} + F_6^{(0)}(-1 + F_9^{(0)})))k^2 - D_2^{(0)}(F_6^{(1)} - F_6^{(0)} \\ & + F_8^{(0)})(D_3^{(0)^2} + k^2) - (F_6^{(0)} + F_8^{(-1)})(2D_2^{(0)}D_3^{(1)}D_3^{(0)} \\ & + D_2^{(1)}(D_3^{(0)^2} + k^2))\ ,\end{aligned}$$

$$E_8^{(0)} = F_7^{(-1)}(-D_1^{(0)^2} + k^2)R^{(1)}(\rho_s - \rho_f)\,,$$
$$E_8^{(1)} = (F_7^{(-1)}(-2D_1^{(1)}D_1^{(0)} + D_1^{(0)^2} - k^2)R^{(1)} + (-D_1^{(0)^2} + k^2)(F_5^{(0)}Q^{(1)} + F_7^{(0)}R^{(1)}))(\rho_s - \rho_f)\,,$$
$$E_9^{(0)} = F_7^{(-1)}(-D_1^{(0)^2} + k^2)R^{(1)}\rho_s\,,$$
$$E_9^{(1)} = -2D_1^{(1)}D_1^{(0)}F_7^{(-1)}R^{(1)}\rho_s + k^2(F_7^{(0)}R^{(1)}\rho_s - F_7^{(-1)}(R^{(1)}\rho_s + Q^{(1)}\rho_f) + F_5^{(0)}(Q^{(1)}\rho_s - \rho_f\lambda^{(0)})) + D_1^{(0)^2}(-F_5^{(0)}Q^{(1)}\rho_s + F_7^{(-1)}R^{(1)}\rho_s - F_7^{(0)}R^{(1)}\rho_s + F_7^{(-1)}Q^{(1)}\rho_f + F_5^{(0)}\rho_f(\lambda^{(0)} + 2\mu))\,,$$
$$E_{10}^{(0)} = F_8^{(-1)}(-D_2^{(0)^2} + k^2)R^{(1)}\rho_f\,,$$
$$E_{10}^{(1)} = \rho_f(-2D_2^{(1)}D_2^{(0)}F_8^{(-1)}R^{(1)} - k^2(-F_8^{(0)}R^{(1)} + F_8^{(-1)}(Q^{(1)} + R^{(1)}) + F_6^{(0)}(-Q^{(1)} + \lambda^{(0)})) + D_2^{(0)^2}(-F_8^{(0)}R^{(1)} + F_8^{(-1)}(Q^{(1)} + R^{(1)}) + F_6^{(0)}(-Q^{(1)} + \lambda^{(0)} + 2\mu)))\,,$$
$$E_{11}^{(0)} = F_7^{(-1)}(-D_1^{(0)^2} + k^2)R^{(1)}\rho_f\,,$$
$$E_{11}^{(1)} = \rho_f(-2D_1^{(1)}D_1^{(0)}F_7^{(-1)}R^{(1)} - k^2(-F_7^{(0)}R^{(1)} + F_7^{(-1)}(Q^{(1)} + R^{(1)}) + F_5^{(0)}(-Q^{(1)} + \lambda^{(0)})) + D_1^{(0)^2}(-F_7^{(0)}R^{(1)} + F_7^{(-1)}(Q^{(1)} + R^{(1)}) + F_5^{(0)}(-Q^{(1)} + \lambda^{(0)} + 2\mu)))\,,$$
$$E_{12}^{(0)} = 2D_1^{(0)}F_5^{(0)}F_8^{(-1)}(D_2^{(0)^2} - k^2)R^{(1)}\,,$$
$$E_{12}^{(1)} = 2(F_8^{(-1)}(2D_1^{(0)}D_2^{(1)}D_2^{(0)}F_5^{(0)} + (D_1^{(0)}F_5^{(1)} + D_1^{(1)}F_5^{(0)})(D_2^{(0)^2} - k^2))R^{(1)} + D_1^{(0)}F_5^{(0)}(D_2^{(0)^2} - k^2)(F_6^{(0)}Q^{(1)} + F_8^{(0)}R^{(1)}))\,,$$
$$E_{13}^{(0)} = 2D_2^{(0)}F_6^{(0)}F_7^{(-1)}(D_1^{(0)^2} - k^2)R^{(1)}\,,$$
$$E_{13}^{(1)} = 2(F_7^{(-1)}(2D_1^{(1)}D_1^{(0)}D_2^{(0)}F_6^{(0)} + (D_2^{(0)}F_6^{(1)} + D_2^{(1)}F_6^{(0)})(D_1^{(0)^2} - k^2))R^{(1)} + D_2^{(0)}F_6^{(0)}(D_1^{(0)^2} - k^2)(F_5^{(0)}Q^{(1)} + F_7^{(0)}R^{(1)}))\,,$$
$$E_{14}^{(0)} = 0\,,\quad E_{15}^{(0)} = 0\,,\quad E_{16}^{(0)} = 0\,,$$
$$E_{14}^{(1)} = \rho_f\,,\quad E_{15}^{(1)} = \rho_f\,,\quad E_{16}^{(1)} = 0\,,$$
$$E_{17}^{(0)} = 2D_1^{(0)}F_5^{(0)}F_7^{(-1)}(D_1^{(0)^2} - k^2)R^{(1)}\,,$$
$$E_{17}^{(1)} = 2(F_7^{(-1)}(2D_1^{(1)}D_1^{(0)^2}F_5^{(0)} + (D_1^{(0)}F_5^{(1)} + D_1^{(1)}F_5^{(0)})(D_1^{(0)^2} - k^2))R^{(1)} + D_1^{(0)}F_5^{(0)}(D_1^{(0)^2} - k^2)(F_5^{(0)}Q^{(1)} + F_7^{(0)}R^{(1)}))\,,$$
$$E_{18}^{(0)} = 2D_2^{(0)}F_6^{(0)}F_8^{(-1)}(D_2^{(0)^2} - k^2)R^{(1)}\,,$$
$$E_{18}^{(1)} = 2(F_8^{(-1)}(2D_2^{(1)}D_2^{(0)^2}F_6^{(0)} + (D_2^{(0)}F_6^{(1)} + D_2^{(1)}F_6^{(0)})(D_2^{(0)^2} - k^2))R^{(1)} + D_2^{(0)}F_6^{(0)}(D_2^{(0)^2} - k^2)(F_6^{(0)}Q^{(1)} + F_8^{(0)}R^{(1)}))\,,$$
$$E_{19}^{(0)} = F_7^{(-1)}(D_1^{(0)^2} - k^2)(D_3^{(0)^2} + k^2)R^{(1)}\,,$$
$$E_{19}^{(1)} = (F_7^{(-1)}(2D_3^{(1)}D_3^{(0)}(D_1^{(0)^2} - k^2) + 2D_1^{(1)}D_1^{(0)}(D_3^{(0)^2} + k^2))R^{(1)} + (D_1^{(0)^2} - k^2)(D_3^{(0)^2} + k^2)(F_5^{(0)}Q^{(1)} + F_7^{(0)}R^{(1)}))\,,$$
$$E_{20}^{(0)} = F_8^{(-1)}(D_2^{(0)^2} - k^2)(D_3^{(0)^2} + k^2)R^{(1)}\,,$$
$$E_{20}^{(1)} = (F_8^{(-1)}(2D_3^{(1)}D_3^{(0)}(D_2^{(0)^2} - k^2) + 2D_2^{(1)}D_2^{(0)}(D_3^{(0)^2} + k^2))R^{(1)} + (D_2^{(0)^2} - k^2)(D_3^{(0)^2} + k^2)(F_6^{(0)}Q^{(1)} + F_8^{(0)}R^{(1)}))\,,$$
$$E_{21}^{(0)} = 2D_1^{(0)}F_5^{(0)}\,,\quad E_{21}^{(1)} = (2D_1^{(0)}F_5^{(1)} + 2D_1^{(1)}F_5^{(0)})\,,$$
$$E_{22}^{(0)} = 2D_2^{(0)}F_6^{(0)}\,,\quad E_{22}^{(1)} = (2D_2^{(0)}F_6^{(1)} + 2D_2^{(1)}F_6^{(0)})\,,$$
$$E_{23}^{(0)} = D_3^{(0)^2} + k^2\,,\quad E_{23}^{(1)} = 2D_3^{(1)}D_3^{(0)}\,,$$

$$T_1^{(0)} = 2E_1^{(0)}(E_{13}^{(0)}E_{23}^{(0)}E_2^{(0)}(1 - \cosh(D_2^{(0)}h)\cosh(D_3^{(0)}h))\sinh(D_1^{(0)}h) + E_{12}^{(0)}E_{23}^{(0)}E_2^{(0)}(-1 + \cosh(D_1^{(0)}h)\cosh(D_3^{(0)}h))\sinh(D_2^{(0)}h) + E_{12}^{(0)}E_{13}^{(0)}E_1^{(0)}(1 - \cosh(D_1^{(0)}h)\cosh(D_2^{(0)}h))\sinh(D_3^{(0)}h)) + ((E_{12}^{(0)^2} + E_{13}^{(0)^2})E_1^{(0)^2} + E_{23}^{(0)^2}E_2^{(0)^2}) \times \sinh(D_1^{(0)}h)\sinh(D_2^{(0)}h)\sinh(D_3^{(0)}h)\,,$$
$$T_1^{(1)} = D_1^{(1)}h\cosh(D_1^{(0)}h)(-2E_{13}^{(0)}E_1^{(0)}E_{23}^{(0)}E_2^{(0)} \times (-1 + \cosh(D_2^{(0)}h)\cosh(D_3^{(0)}h)) + ((E_{12}^{(0)^2} + E_{13}^{(0)^2})E_1^{(0)^2} + E_{23}^{(0)^2}E_2^{(0)^2}) \times \sinh(D_2^{(0)}h)\sinh(D_3^{(0)}h)) + \sinh(D_1^{(0)}h) \times (D_3^{(1)}((E_{12}^{(0)^2} + E_{13}^{(0)^2})E_1^{(0)^2} + E_{23}^{(0)^2}E_2^{(0)^2}) \times h\cosh(D_3^{(0)}h)\sinh(D_2^{(0)}h) + (D_2^{(1)}((E_{12}^{(0)^2} + E_{13}^{(0)^2})E_1^{(0)^2} + E_{23}^{(0)^2}E_2^{(0)^2}) \times h\cosh(D_2^{(0)}h) + 2(E_1^{(0)}(E_{12}^{(0)} \times (E_{12}^{(0)}E_1^{(1)} + E_{12}^{(1)}E_1^{(0)}) + E_{13}^{(0)}(E_{13}^{(0)}E_1^{(1)} + E_{13}^{(1)}E_1^{(0)})) + E_{23}^{(0)}E_2^{(0)}(E_{23}^{(0)}E_2^{(1)} + E_{23}^{(1)}E_2^{(0)}))\sinh(D_2^{(0)}h))\sinh(D_3^{(0)}h) - 2((E_1^{(0)}E_{23}^{(0)}(E_{13}^{(0)}E_2^{(1)} + E_{13}^{(1)}E_2^{(0)}) + E_2^{(0)}E_{13}^{(0)}(E_1^{(0)}E_{23}^{(1)} + E_1^{(1)}E_{23}^{(0)}))(-1 + \cosh(D_2^{(0)}h)\cosh(D_3^{(0)}h)) + E_{13}^{(0)}E_1^{(0)}E_{23}^{(0)}E_2^{(0)}h(D_2^{(1)}\cosh(D_3^{(0)}h)\sinh(D_2^{(0)}h) + D_3^{(1)}\cosh(D_2^{(0)}h) \times \sinh(D_3^{(0)}h)))) + 2((E_{12}^{(0)}E_1^{(1)} + E_{12}^{(1)}E_1^{(0)})(E_{23}^{(0)}E_2^{(0)}(-1 + \cosh(D_1^{(0)}h) \times \cosh(D_3^{(0)}h))\sinh(D_2^{(0)}h) + E_{13}^{(0)}E_1^{(0)}(1 - \cosh(D_1^{(0)}h)\cosh(D_2^{(0)}h)) \times \sinh(D_3^{(0)}h)) + E_{12}^{(0)}E_1^{(0)}(D_3^{(1)}E_{13}^{(0)}E_1^{(0)}h \times (1 - \cosh(D_1^{(0)}h)\cosh(D_2^{(0)}h)) \times \cosh(D_3^{(0)}h) + D_2^{(1)}E_{23}^{(0)}E_2^{(0)}h\cosh(D_2^{(0)}h) \times (-1 + \cosh(D_1^{(0)}h)\cosh(D_3^{(0)}h)) + ((E_{13}^{(0)}E_1^{(1)} + E_{13}^{(1)}E_1^{(0)})(1 - \cosh(D_1^{(0)}h)\cosh(D_2^{(0)}h)) - E_{13}^{(0)}E_1^{(0)}h(D_1^{(1)} \times \cosh(D_2^{(0)}h)\sinh(D_1^{(0)}h) + D_2^{(1)}\cosh(D_1^{(0)}h) \times \sinh(D_2^{(0)}h)))\sinh(D_3^{(0)}h) + \sinh(D_2^{(0)}h)((E_{23}^{(0)}E_2^{(1)} + E_{23}^{(1)}E_2^{(0)}) \times (-1 + \cosh(D_1^{(0)}h)\cosh(D_3^{(0)}h)) + E_{23}^{(0)}E_2^{(0)}h(D_1^{(1)}\cosh(D_3^{(0)}h)\sinh(D_1^{(0)}h) + D_3^{(1)}\cosh(D_1^{(0)}h)\sinh(D_3^{(0)}h)))))\,,$$
$$T_2^{(0)} = E_1^{(0)}((E_{17}^{(0)}E_4^{(0)}E_7^{(0)} + E_{18}^{(0)}E_6^{(0)}E_9^{(0)}) \times (-1 + \cosh(D_1^{(0)}h)\cosh(D_2^{(0)}h)) + E_{20}^{(0)}E_5^{(0)}E_9^{(0)}(-1 + \cosh(D_1^{(0)}h)\cosh(D_3^{(0)}h)) - E_{19}^{(0)}E_4^{(0)}E_5^{(0)}(-1 + \cosh(D_2^{(0)}h)\cosh(D_3^{(0)}h))) + E_1^{(0)}((E_{17}^{(0)}E_3^{(0)}E_7^{(0)} + E_{18}^{(0)}E_6^{(0)}E_8^{(0)})(1 - \cosh(D_1^{(0)}h)\cosh(D_2^{(0)}h))\cosh(D_3^{(0)}h) - E_{20}^{(0)}E_5^{(0)}E_8^{(0)}\cosh(D_2^{(0)}h)(-1 + \cosh(D_1^{(0)}h)\cosh(D_3^{(0)}h)) + E_{19}^{(0)}E_3^{(0)}E_5^{(0)}\cosh(D_1^{(0)}h) \times (-1 + \cosh(D_2^{(0)}h) \times \cosh(D_3^{(0)}h))) - E_1^{(0)}(E_{12}^{(0)}E_4^{(0)}E_6^{(0)} + E_{13}^{(0)}E_7^{(0)}E_9^{(0)} + (E_{12}^{(0)}E_3^{(0)}E_6^{(0)}$$

$$
\begin{aligned}
&+ E_{13}^{(0)}E_7^{(0)}E_8^{(0)})\cosh(D_3^{(0)}h))\sinh(D_1^{(0)}h)\sinh(D_2^{(0)}h)\\
&+ E_{23}^{(0)}E_2^{(0)}E_7^{(0)}(E_9^{(0)}\\
&- E_8^{(0)}\cosh(D_2^{(0)}h))\sinh(D_1^{(0)}h)\sinh(D_3^{(0)}h) - E_{23}^{(0)}E_2^{(0)}E_6^{(0)}(E_4^{(0)}\\
&+ E_3^{(0)}\cosh(D_1^{(0)}h))\sinh(D_2^{(0)}h)\sinh(D_3^{(0)}h)\ ,\\
T_2^{(1)} &= E_1^{(1)}((E_{17}^{(0)}E_4^{(0)}E_7^{(0)} + E_{18}^{(0)}E_6^{(0)}E_9^{(0)})\\
&\times(-1+\cosh(D_1^{(0)}h)\cosh(D_2^{(0)}h))\\
&+ E_{20}^{(0)}E_5^{(0)}E_9^{(0)}(-1+\cosh(D_1^{(0)}h)\cosh(D_3^{(0)}h))\\
&- E_{19}^{(0)}E_4^{(0)}E_5^{(0)}(-1+\cosh(D_2^{(0)}h)\\
&\times\cosh(D_3^{(0)}h))) + E_1^{(1)}(E_{20}^{(0)}E_5^{(0)}E_8^{(0)}\cosh(D_2^{(0)}h)\\
&+ (E_{17}^{(0)}E_3^{(0)}E_7^{(0)} + E_{18}^{(0)}E_6^{(0)}E_8^{(0)})\\
&\times\cosh(D_3^{(0)}h) + \cosh(D_1^{(0)}h)(-E_{19}^{(0)}E_3^{(0)}E_5^{(0)}\\
&+ (E_{19}^{(0)}E_3^{(0)}E_5^{(0)} - E_{17}^{(0)}E_3^{(0)}E_7^{(0)}\\
&- (E_{20}^{(0)}E_5^{(0)} + E_{18}^{(0)}E_6^{(0)})E_8^{(0)})\cosh(D_2^{(0)}h)\cosh(D_3^{(0)}h)))\\
&- D_2^{(1)}E_1^{(0)}(E_{12}^{(0)}E_4^{(0)}E_6^{(0)}\\
&+ E_{13}^{(0)}E_7^{(0)}E_9^{(0)})h\cosh(D_2^{(0)}h)\sinh(D_1^{(0)}h)\\
&+ D_3^{(1)}E_{23}^{(0)}E_2^{(0)}E_7^{(0)}E_9^{(0)}h\cosh(D_3^{(0)}h)\\
&\times\sinh(D_1^{(0)}h) - (D_3^{(1)}E_{23}^{(0)}E_2^{(0)}E_7^{(0)}E_8^{(0)}\\
&+ D_2^{(1)}E_1^{(0)}(E_{12}^{(0)}E_3^{(0)}E_6^{(0)} + E_{13}^{(0)}E_7^{(0)}E_8^{(0)}))\\
&\times h\cosh(D_2^{(0)}h)\cosh(D_3^{(0)}h)\sinh(D_1^{(0)}h)\\
&- D_3^{(1)}E_{23}^{(0)}E_2^{(0)}E_4^{(0)}E_6^{(0)}h\cosh(D_3^{(0)}h)\\
&\times\sinh(D_2^{(0)}h) + D_3^{(1)}E_{23}^{(0)}E_2^{(0)}E_3^{(0)}E_6^{(0)}h\\
&\times\cosh(D_1^{(0)}h)\cosh(D_3^{(0)}h)\sinh(D_2^{(0)}h)\\
&- (D_1^{(1)}E_1^{(0)}(E_{12}^{(0)}E_4^{(0)}E_6^{(0)} + E_{13}^{(0)}E_7^{(0)}E_9^{(0)})h\cosh(D_1^{(0)}h)\\
&+ (E_1^{(0)}((E_{12}^{(0)}(E_4^{(0)}E_6^{(1)}\\
&+ E_4^{(1)}E_6^{(0)}) + E_{12}^{(1)}E_4^{(0)}E_6^{(0)} + E_{13}^{(0)}(E_7^{(0)}E_9^{(1)} + E_7^{(1)}E_9^{(0)})\\
&+ E_{13}^{(1)}E_7^{(0)}E_9^{(0)}))\\
&+ E_1^{(1)}(E_{12}^{(0)}E_4^{(0)}E_6^{(0)} + E_{13}^{(0)}E_7^{(0)}E_9^{(0)}))\sinh(D_1^{(0)}h))\sinh(D_2^{(0)}h)\\
&+ (D_1^{(1)}E_{23}^{(0)}E_2^{(0)}\\
&\times E_7^{(0)}E_9^{(0)}h\cosh(D_1^{(0)}h) + (-E_{12}^{(0)}E_{14}^{(1)}{E_1^{(0)}}^2E_5^{(0)}\\
&+ E_{23}^{(0)}E_2^{(0)}(E_7^{(0)}E_9^{(1)} + E_7^{(1)}E_9^{(0)})\\
&+ (E_{23}^{(0)}E_2^{(1)} + E_{23}^{(1)}E_2^{(0)})E_7^{(0)}E_9^{(0)})\sinh(D_1^{(0)}h))\\
&\times\sinh(D_3^{(0)}h) + (-D_2^{(1)}E_{23}^{(0)}E_2^{(0)}E_4^{(0)}E_6^{(0)}\\
&\times h\cosh(D_2^{(0)}h) + (E_{13}^{(0)}E_{14}^{(1)}{E_1^{(0)}}^2E_5^{(0)} - E_2^{(0)}E_4^{(0)}(E_{23}^{(0)}E_6^{(1)}\\
&+ E_{23}^{(1)}E_6^{(0)}) - E_{23}^{(0)}(E_2^{(0)}E_4^{(1)}\\
&+ E_2^{(1)}E_4^{(0)})E_6^{(0)})\sinh(D_2^{(0)}h))\sinh(D_3^{(0)}h)\\
&+ (D_1^{(1)}E_{23}^{(0)}E_2^{(0)}E_3^{(0)}E_6^{(0)}h\sinh(D_1^{(0)}h)\\
&\times\sinh(D_2^{(0)}h) + \cosh(D_1^{(0)}h)(D_2^{(1)}E_{23}^{(0)}E_2^{(0)}E_3^{(0)}E_6^{(0)}h\cosh(D_2^{(0)}h)\\
&+ (-E_{13}^{(0)}E_{16}^{(1)}\\
&\times{E_1^{(0)}}^2E_5^{(0)} + E_{23}^{(0)}E_2^{(0)}(E_3^{(0)}E_6^{(1)} + E_3^{(1)}E_6^{(0)}) + (E_{23}^{(0)}E_2^{(1)}\\
&+ E_{23}^{(1)}E_2^{(0)})E_3^{(0)}E_6^{(0)})\\
&\times\sinh(D_2^{(0)}h)))\sinh(D_3^{(0)}h) + (-D_1^{(1)}E_{23}^{(0)}E_2^{(0)}E_7^{(0)}E_8^{(0)}h\\
&\times\cosh(D_1^{(0)}h)\cosh(D_2^{(0)}h)\\
&+ \sinh(D_1^{(0)}h)((E_{12}^{(0)}E_{16}^{(1)}{E_1^{(0)}}^2E_5^{(0)} - E_{23}^{(0)}E_2^{(0)}(E_7^{(0)}E_8^{(1)}\\
&+ E_7^{(1)}E_8^{(0)}) - (E_{23}^{(0)}E_2^{(1)}\\
&+ E_{23}^{(1)}E_2^{(0)})E_7^{(0)}E_8^{(0)})\cosh(D_2^{(0)}h) - D_2^{(1)}E_{23}^{(0)}E_2^{(0)}E_7^{(0)}E_8^{(0)}h\\
&\times\sinh(D_2^{(0)}h)))\sinh(D_3^{(0)}h)\\
&+ \sinh(D_2^{(0)}h)(D_1^{(1)}E_1^{(0)}(E_{12}^{(0)}E_3^{(0)}E_6^{(0)}\\
&+ E_{13}^{(0)}E_7^{(0)}E_8^{(0)})h\cosh(D_1^{(0)}h)\cosh(D_3^{(0)}h)\\
&+ \sinh(D_1^{(0)}h)((E_1^{(0)}(E_{12}^{(0)}(E_3^{(0)}E_6^{(1)} + E_3^{(1)}E_6^{(0)})\\
&+ E_{12}^{(1)}E_3^{(0)}E_6^{(0)} + E_{13}^{(1)}E_7^{(0)}E_8^{(0)}\\
&+ E_{13}^{(0)}(E_7^{(0)}E_8^{(1)} + E_7^{(1)}E_8^{(0)}))\\
&+ E_1^{(1)}(E_{12}^{(0)}E_3^{(0)}E_6^{(0)} + E_{13}^{(0)}E_7^{(0)}E_8^{(0)}))\cosh(D_3^{(0)}h)\\
&+ D_3^{(1)}E_1^{(0)}(E_{12}^{(0)}E_3^{(0)}E_6^{(0)} + E_{13}^{(0)}E_7^{(0)}E_8^{(0)})h\sinh(D_3^{(0)}h)))\\
&+ E_1^{(0)}((E_{17}^{(0)}(E_4^{(0)}E_7^{(1)}\\
&+ E_4^{(1)}E_7^{(0)}) + E_{18}^{(0)}(E_6^{(0)}E_9^{(1)} + E_6^{(1)}E_9^{(0)})\\
&+ E_{17}^{(1)}E_4^{(0)}E_7^{(0)} + E_{18}^{(1)}E_6^{(0)}E_9^{(0)})(-1\\
&+ \cosh(D_1^{(0)}h)\cosh(D_2^{(0)}h)) + (E_{14}^{(1)}E_{21}^{(0)}E_2^{(0)}E_7^{(0)}\\
&- E_{20}^{(1)}E_5^{(0)}E_9^{(0)} - E_{20}^{(0)}(E_5^{(0)}E_9^{(1)}\\
&+ E_5^{(1)}E_9^{(0)}))(1-\cosh(D_1^{(0)}h)\cosh(D_3^{(0)}h))\\
&- (E_{19}^{(0)}(E_4^{(0)}E_5^{(1)} + E_4^{(1)}E_5^{(0)}) + E_{19}^{(1)}\\
&\times E_4^{(0)}E_5^{(0)} - E_{14}^{(1)}E_{22}^{(0)}E_2^{(0)}E_6^{(0)})\\
&\times(-1+\cosh(D_2^{(0)}h)\cosh(D_3^{(0)}h)) + (E_{17}^{(0)}E_4^{(0)}E_7^{(0)}\\
&+ E_{18}^{(0)}E_6^{(0)}E_9^{(0)})h(D_1^{(1)}\cosh(D_2^{(0)}h)\sinh(D_1^{(0)}h)\\
&+ D_2^{(1)}\cosh(D_1^{(0)}h)\sinh(D_2^{(0)}h))\\
&+ E_{20}^{(0)}E_5^{(0)}E_9^{(0)}h(D_1^{(1)}\cosh(D_3^{(0)}h)\sinh(D_1^{(0)}h)\\
&+ D_3^{(1)}\cosh(D_1^{(0)}h)\sinh(D_3^{(0)}h))\\
&- E_{19}^{(0)}E_4^{(0)}E_5^{(0)}h(D_2^{(1)}\cosh(D_3^{(0)}h)\sinh(D_2^{(0)}h)\\
&+ D_3^{(1)}\cosh(D_2^{(0)}h)\sinh(D_3^{(0)}h)))\\
&+ E_1^{(0)}((-1+\cosh(D_2^{(0)}h)\cosh(D_3^{(0)}h))((E_{19}^{(0)}(E_3^{(0)}E_5^{(1)}\\
&+ E_3^{(1)}E_5^{(0)}) + E_{19}^{(1)}E_3^{(0)}E_5^{(0)}\\
&- E_{16}^{(1)}E_{22}^{(0)}E_2^{(0)}E_6^{(0)})\cosh(D_1^{(0)}h)\\
&+ D_1^{(1)}E_{19}^{(0)}E_3^{(0)}E_5^{(0)}h\sinh(D_1^{(0)}h)) + (-1\\
&+ \cosh(D_1^{(0)}h)\cosh(D_3^{(0)}h))((E_{16}^{(1)}E_{21}^{(0)}E_2^{(0)}E_7^{(0)}\\
&- E_{20}^{(1)}E_5^{(0)}E_8^{(0)} - E_{20}^{(0)}(E_5^{(0)}E_8^{(1)}\\
&+ E_5^{(1)}E_8^{(0)}))\cosh(D_2^{(0)}h) - D_2^{(1)}E_{20}^{(0)}E_5^{(0)}E_8^{(0)}h\sinh(D_2^{(0)}h))\\
&+ \cosh(D_3^{(0)}h)((E_{17}^{(0)}\\
&\times(E_3^{(0)}E_7^{(1)} + E_3^{(1)}E_7^{(0)}) + E_{18}^{(0)}(E_6^{(0)}E_8^{(1)} + E_6^{(1)}E_8^{(0)})\\
&+ E_{17}^{(1)}E_3^{(0)}E_7^{(0)} + E_{18}^{(1)}E_6^{(0)}E_8^{(0)})\\
&\times(1-\cosh(D_1^{(0)}h)\cosh(D_2^{(0)}h)) - (E_{17}^{(0)}E_3^{(0)}E_7^{(0)}\\
&+ E_{18}^{(0)}E_6^{(0)}E_8^{(0)})h(D_1^{(1)}\cosh(D_2^{(0)}h)\\
&\times\sinh(D_1^{(0)}h) + D_2^{(1)}\cosh(D_1^{(0)}h)\sinh(D_2^{(0)}h)))\\
&+ D_3^{(1)}(E_{17}^{(0)}E_3^{(0)}E_7^{(0)} + E_{18}^{(0)}E_6^{(0)}E_8^{(0)})\\
&\times h(1-\cosh(D_1^{(0)}h)\cosh(D_2^{(0)}h))\sinh(D_3^{(0)}h)\\
&- E_{20}^{(0)}E_5^{(0)}E_8^{(0)}h\cosh(D_2^{(0)}h)\\
&\times(D_1^{(1)}\cosh(D_3^{(0)}h)\sinh(D_1^{(0)}h) + D_3^{(1)}\cosh(D_1^{(0)}h)\sinh(D_3^{(0)}h))\\
&+ E_{19}^{(0)}E_3^{(0)}E_5^{(0)}\\
&\times h\cosh(D_1^{(0)}h)(D_2^{(1)}\cosh(D_3^{(0)}h)\sinh(D_2^{(0)}h)\\
&+ D_3^{(1)}\cosh(D_2^{(0)}h)\sinh(D_3^{(0)}h)))\ ,\\
T_3^{(0)} &= E_1^{(0)}\cosh(D_3^{(0)}h)(E_{11}^{(0)}E_{18}^{(0)}E_6^{(0)} + E_{10}^{(0)}E_{17}^{(0)}E_7^{(0)}\\
&+ (E_{10}^{(0)}E_{12}^{(0)}E_6^{(0)} + E_{11}^{(0)}E_{13}^{(0)}E_7^{(0)})
\end{aligned}
$$

$$
\begin{aligned}
&\times \sinh(D_1^{(0)}h)\sinh(D_2^{(0)}h)) + E_{11}^{(0)}\cosh(D_2^{(0)}h)(E_1^{(0)}E_{20}^{(0)}E_5^{(0)}\\
&- E_{23}^{(0)}E_2^{(0)}E_7^{(0)}\\
&\times \sinh(D_1^{(0)}h)\sinh(D_3^{(0)}h)) + \cosh(D_1^{(0)}h)(-E_{10}^{(0)}E_{19}^{(0)}E_1^{(0)}E_5^{(0)}\\
&- E_1^{(0)}((-E_{10}^{(0)}E_{19}^{(0)}\\
&+ E_{11}^{(0)}E_{20}^{(0)})E_5^{(0)} + E_{11}^{(0)}E_{18}^{(0)}E_6^{(0)}\\
&+ E_{10}^{(0)}E_{17}^{(0)}E_7^{(0)})\cosh(D_2^{(0)}h)\cosh(D_3^{(0)}h)\\
&+ E_{10}^{(0)}E_{23}^{(0)}E_2^{(0)}E_6^{(0)}\sinh(D_2^{(0)}h)\sinh(D_3^{(0)}h))\,,\\
T_3^{(1)} &= E_1^{(1)}(E_{11}^{(0)}E_{20}^{(0)}E_5^{(0)}\cosh(D_2^{(0)}h) + (E_{11}^{(0)}E_{18}^{(0)}E_6^{(0)}\\
&+ E_{10}^{(0)}E_{17}^{(0)}E_7^{(0)})\cosh(D_3^{(0)}h)\\
&+ \cosh(D_1^{(0)}h)(-E_{10}^{(0)}E_{19}^{(0)}E_5^{(0)} - ((-E_{10}^{(0)}E_{19}^{(0)}\\
&+ E_{11}^{(0)}E_{20}^{(0)})E_5^{(0)} + E_{11}^{(0)}E_{18}^{(0)}E_6^{(0)}\\
&+ E_{10}^{(0)}E_{17}^{(0)}E_7^{(0)})\cosh(D_2^{(0)}h)\cosh(D_3^{(0)}h)))\\
&+ (-D_3^{(1)}E_{11}^{(0)}E_{23}^{(0)}E_2^{(0)}E_7^{(0)} + D_2^{(1)}E_1^{(0)}\\
&\times (E_{10}^{(0)}E_{12}^{(0)}E_6^{(0)} + E_{11}^{(0)}E_{13}^{(0)}E_7^{(0)}))h\\
&\times \cosh(D_2^{(0)}h)\cosh(D_3^{(0)}h)\sinh(D_1^{(0)}h)\\
&+ D_3^{(1)}E_{10}^{(0)}E_{23}^{(0)}E_2^{(0)}E_6^{(0)}h\cosh(D_1^{(0)}h)\cosh(D_3^{(0)}h)\sinh(D_2^{(0)}h)\\
&- (-D_1^{(1)}E_{10}^{(0)}E_{23}^{(0)}E_2^{(0)}\\
&\times E_6^{(0)}h\sinh(D_1^{(0)}h)\sinh(D_2^{(0)}h) - \cosh(D_1^{(0)}h)\\
&\times (D_2^{(1)}E_{10}^{(0)}E_{23}^{(0)}E_2^{(0)}E_6^{(0)}h\cosh(D_2^{(0)}h)\\
&+ (-E_{13}^{(0)}E_{15}^{(1)}E_1^{(0)^2}E_5^{(0)} + E_{10}^{(0)}E_{23}^{(0)}(E_2^{(0)}E_6^{(1)} + E_2^{(1)}E_6^{(0)})\\
&+ (E_{10}^{(0)}E_{23}^{(1)} + E_{10}^{(1)}E_{23}^{(0)})E_2^{(0)}\\
&\times E_6^{(0)})\sinh(D_2^{(0)}h)))\sinh(D_3^{(0)}h)\\
&+ (-D_1^{(1)}E_{11}^{(0)}E_{23}^{(0)}E_2^{(0)}E_7^{(0)}h\cosh(D_1^{(0)}h)\cosh(D_2^{(0)}h)\\
&+ \sinh(D_1^{(0)}h)((E_{12}^{(0)}E_{15}^{(1)}E_1^{(0)^2}E_5^{(0)} - E_{23}^{(0)}E_2^{(0)}(E_{11}^{(0)}E_7^{(1)}\\
&+ E_{11}^{(1)}E_7^{(0)}) - E_{11}^{(0)}(E_{23}^{(0)}E_2^{(1)}\\
&+ E_{23}^{(1)}E_2^{(0)})E_7^{(0)})\cosh(D_2^{(0)}h)\\
&- D_2^{(1)}E_{11}^{(0)}E_{23}^{(0)}E_2^{(0)}E_7^{(0)}h\sinh(D_2^{(0)}h)))\sinh(D_3^{(0)}h)\\
&+ \sinh(D_2^{(0)}h)(D_1^{(1)}E_1^{(0)}(E_{10}^{(0)}E_{12}^{(0)}E_6^{(0)}\\
&+ E_{11}^{(0)}E_{13}^{(0)}E_7^{(0)})h\cosh(D_1^{(0)}h)\cosh(D_3^{(0)}h)\\
&+ \sinh(D_1^{(0)}h)((E_1^{(0)}(E_{10}^{(0)}(E_{12}^{(0)}E_6^{(1)} + E_{12}^{(1)}E_6^{(0)})\\
&+ E_{10}^{(1)}E_{12}^{(0)}E_6^{(0)} + E_{11}^{(0)}E_{13}^{(0)}E_7^{(1)}\\
&+ (E_{11}^{(0)}E_{13}^{(1)} + E_{11}^{(1)}E_{13}^{(0)})E_7^{(0)})\\
&+ E_1^{(1)}(E_{10}^{(0)}E_{12}^{(0)}E_6^{(0)} + E_{11}^{(0)}E_{13}^{(0)}E_7^{(0)}))\cosh(D_3^{(0)}h)\\
&+ D_3^{(1)}E_1^{(0)}(E_{10}^{(0)}E_{12}^{(0)}E_6^{(0)} + E_{11}^{(0)}E_{13}^{(0)}E_7^{(0)})h\\
&\times \sinh(D_3^{(0)}h))) + E_1^{(0)}((-1+\cosh(D_2^{(0)}h)\\
&\times \cosh(D_3^{(0)}h))((E_{10}^{(0)}(E_{19}^{(0)}E_5^{(1)} + E_{19}^{(1)}E_5^{(0)})\\
&+ E_{10}^{(1)}E_{19}^{(0)}E_5^{(0)} - E_{15}^{(1)}E_{22}^{(0)}E_2^{(0)}E_6^{(0)})\\
&\times \cosh(D_1^{(0)}h) + D_1^{(1)}E_{10}^{(0)}E_{19}^{(0)}E_5^{(0)}h\sinh(D_1^{(0)}h))\\
&- (-1+\cosh(D_1^{(0)}h)\cosh(D_3^{(0)}h))\\
&\times ((E_{11}^{(0)}(E_{20}^{(0)}E_5^{(1)} + E_{20}^{(1)}E_5^{(0)}) + E_{11}^{(1)}E_{20}^{(0)}E_5^{(0)}\\
&- E_{15}^{(1)}E_{21}^{(0)}E_2^{(0)}E_7^{(0)})\cosh(D_2^{(0)}h)\\
&+ D_2^{(1)}E_{11}^{(0)}E_{20}^{(0)}E_5^{(0)}h\sinh(D_2^{(0)}h))\\
&+ \cosh(D_3^{(0)}h)((E_{11}^{(0)}(E_{18}^{(0)}E_6^{(1)} + E_{18}^{(1)}E_6^{(0)})\\
&+ E_{11}^{(1)}E_{18}^{(0)}E_6^{(0)} + E_{10}^{(0)}E_{17}^{(0)}E_7^{(1)} + (E_{10}^{(0)}E_{17}^{(1)}\\
&+ E_{10}^{(1)}E_{17}^{(0)})E_7^{(0)})(1-\cosh(D_1^{(0)}h)\\
&\times \cosh(D_2^{(0)}h)) - (E_{11}^{(0)}E_{18}^{(0)}E_6^{(0)} + E_{10}^{(0)}E_{17}^{(0)}E_7^{(0)})h\\
&\times (D_1^{(1)}\cosh(D_2^{(0)}h)\sinh(D_1^{(0)}h)\\
&+ D_2^{(1)}\cosh(D_1^{(0)}h)\sinh(D_2^{(0)}h))) + D_3^{(1)}(E_{11}^{(0)}E_{18}^{(0)}E_6^{(0)}\\
&+ E_{10}^{(0)}E_{17}^{(0)}E_7^{(0)})h(1\\
&- \cosh(D_1^{(0)}h)\cosh(D_2^{(0)}h))\sinh(D_3^{(0)}h)\\
&- E_{11}^{(0)}E_{20}^{(0)}E_5^{(0)}h\cosh(D_2^{(0)}h)(D_1^{(1)}\\
&\times \cosh(D_3^{(0)}h)\sinh(D_1^{(0)}h) + D_3^{(1)}\cosh(D_1^{(0)}h)\sinh(D_3^{(0)}h))\\
&+ E_{10}^{(0)}E_{19}^{(0)}E_5^{(0)}\\
&\times h\cosh(D_1^{(0)}h)(D_2^{(1)}\cosh(D_3^{(0)}h)\sinh(D_2^{(0)}h)\\
&+ D_3^{(1)}\cosh(D_2^{(0)}h)\sinh(D_3^{(0)}h)))\,.
\end{aligned}
$$

References

[1] L.G. Bennetts, V.A. Squire, On the calculation of an attenuation coefficient for transects of ice-covered ocean, Proc. R. Soc. Lond. Ser. A Math. Phys. Eng. Sci. 468 (2012) 136–162.

[2] A.L. Kohout, M.H. Meylan, An elastic plate model for wave attenuation and ice floe breaking in the marginal ice zone, J. Geophys. Res. 113 (2008) C09016.

[3] T.D. Williams, L.G. Bennetts, V.A. Squire, D. Dumont, L. Bertino, Wave-ice interactions in the marginal ice zone. Part 1: Theoretical foundations, Ocean Modell. 71 (2013) 81–91.

[4] G. de Carolis, D. Desiderio, Dispersion and attenuation of gravity waves in ice: a two-layer viscous fluid model with experimental data validation, Phys. Lett. A 305 (2002) 399–412.

[5] J.B. Keller, Gravity waves on ice-covered water, J. Geophys. Res. 103 (1998) 7663–7669.

[6] R. Wang, H.H. Shen, Gravity waves propagating into an ice-covered ocean: A viscoelastic model, J. Geophys. Res. 115 (2010) C06024.

[7] P. Wadhams, V.A. Squire, D.J. Goodman, A.M. Cowan, S.C. Moore, The attenuation rates of ocean waves in the marginal ice zone, J. Geophys. Res. 93 (1988) 6799–6818.

[8] M.J. Doble, J.-R. Bidlot, Wave buoy measurements at the antarctic sea ice edge compared with an enhanced ECMWF WAM: Progress towards global waves-in-ice modeling, Ocean Modell. 70 (2013) 166–173.

[9] T.D. Williams, L.G. Bennetts, V.A. Squire, D. Dumont, L. Bertino, Wave-ice interactions in the marginal ice zone. Part 2: Numerical implementation and sensitivity studies along 1d transects of the ocean surface, Ocean Modell. 71 (2013) 92–101.

[10] W. Craig, P. Guyenne, C. Sulem, Water waves over a random bottom, J. Fluid Mech. 640 (2009) 79–107.

[11] A. de Bouard, W. Craig, O. Diaz-Espinosa, P. Guyenne, C. Sulem, Long wave expansions for water waves over random topography, Nonlinearity 21 (2008) 2143–2178.

[12] C. Fox, V.A. Squire, On the oblique reflexion and transmission of ocean waves at shore fast sea ice, Philos. Trans. R. Soc. Lond. A Math. Phys. Eng. Sci. 347 (1994) 185–218.

[13] A.K. Liu, E. Mollo-Christensen, Wave propagation in a solid ice pack, J. Phys. Oceanogr. 18 (1988) 1702–1712.

[14] V.A. Squire, Of ocean waves and sea-ice revisited, Cold Reg. Sci. Tech. 49 (2007) 110–133.

[15] S. Cheng, W.E. Rogers, J. Thomson, M. Smith, M.J. Doble, P. Wadhams, A.L. Kohout, B. Lund, O.P.G. Persson, C.O. Collins III, S.F. Ackley, F. Montiel, H.H. Shen, Calibrating a viscoelastic sea ice model for wave propagation in the Arctic fall marginal ice zone, J. Geophys. Res. 122 (2017) 8770–8793.

[16] X. Zhao, H.H. Shen, S. Cheng, Modeling ocean wave propagation under sea ice covers, Acta Mech. Sin. 31 (2015) 1–15.

[17] M.J. Doble, G. de Carolis, M.H. Meylan, J.-R. Bidlot, P. Wadhams, Relating wave attenuation to pancake ice thickness, using field measurements and model results, Geophys. Res. Lett. 42 (2015) 4473–4481.

[18] J.L. Buchanan, R.P. Gilbert, A. Wirgin, Y.S. Xu, Marine Acoustics: Direct and Inverse Problems, SIAM, Philadelphia, 2004.

[19] J.L. Buchanan, R.P. Gilbert, Y. Xu, Green's function representation for acoustic pressure over a poroelastic seabed, Appl. Anal. 65 (1997) 57–68.

[20] H. Chen, R.P. Gilbert, P. Guyenne, A Biot model for the determination of material parameters of cancellous bone from acoustic measurements, Inverse Problems 34 (2018) 085009.

[21] R.P. Gilbert, P. Guyenne, G.C. Hsiao, Determination of cancellous bone density using low frequency acoustic measurements, Appl. Anal. 87 (2008) 1213–1225.

[22] R.P. Gilbert, P. Guyenne, M. Shoushani, Recovery of parameters of cancellous bone by acoustic interrogation, Inverse Probl. Sci. Eng. 24 (2016) 284–316.

[23] H. Behera, T. Sahoo, Hydroelastic analysis of gravity wave interaction with submerged horizontal flexible porous plate, J. Fluids Struct. 54 (2015) 643–660.
[24] M.H. Meylan, L.G. Bennetts, M.A. Peter, Water-wave scattering and energy dissipation by a floating porous elastic plate in three dimensions, Wave Motion 70 (2017) 240–250.
[25] C.O. Collins III, W.E. Rogers, B. Lund, An investigation into the dispersion of ocean surface waves in sea ice, Ocean Dyn. 67 (2017) 263–280.
[26] J.E. Mosig, F. Montiel, V.A. Squire, Comparison of viscoelastic-type models for ocean wave attenuation in ice-covered seas, J. Geophys. Res. 120 (2015) 6072–6090.
[27] L. Xu, P. Guyenne, Numerical simulation of three-dimensional nonlinear water waves, J. Comput. Phys. 228 (2009) 8446–8466.
[28] X. Zhao, S. Cheng, H.H. Shen, Nature of wave modes in a coupled viscoelastic layer over water, J. Engng. Mech. 143 (2017) 04017114.
[29] E. Renzi, F. Dias, Hydro-acoustic precursors of gravity waves generated by surface pressure disturbances localised in space and time, J. Fluid Mech. 754 (2014) 250–262.
[30] M.A. Biot, Theory of propagation of elastic waves in a fluid-saturated porous solid. I. Lower frequency range, J. Acoust. Soc. Am. 28 (1956) 168–178.
[31] M.A. Biot, Theory of propagation of elastic waves in a fluid-saturated porous solid. II. Higher frequency range, J. Acoust. Soc. Am. 28 (1956) 179–191.
[32] J.L. Williams, Ultrasonic wave propagation in cancellous and cortical bone: Prediction of some experimental results by Biot's theory, J. Acoust. Soc. Am. 91 (1992) 1106–1112.
[33] R.D. Stoll, T.K. Kan, Reflection of acoustic waves at a water-sediment interface, J. Acoust. Soc. Am. 70 (1981) 149–156.
[34] P. Guyenne, Large-amplitude internal solitary waves in a two-fluid model, C. R. Mec. 334 (2006) 341–346.
[35] P. Guyenne, E.I. Părău, Finite-depth effects on solitary waves in a floating ice sheet, J. Fluids Struct. 49 (2014) 242–262.
[36] G.S. Sammelmann, Biot–stoll model of the high-frequency reflection coefficient of sea ice, J. Acoust. Soc. Am. 94 (1993) 371–385.
[37] K.L. Williams, R.E. Francois, Sea ice elastic moduli: Determination of Biot parameters using in-field velocity measurements, J. Acoust. Soc. Am. 91 (1992) 2627–2636.
[38] R.A. Dalrymple, P.L.-F. Liu, Waves over soft muds: a two-layer fluid model, J. Phys. Oceanogr. 8 (1978) 1121–1131.
[39] P. Guyenne, E.I. Părău, Computations of fully nonlinear hydroelastic solitary waves on deep water, J. Fluid Mech. 713 (2012) 307–329.
[40] P. Guyenne, E.I. Părău, Numerical study of solitary wave attenuation in a fragmented ice sheet, Phys. Rev. Fluids 2 (2017) 034002.
[41] J. Li, A.L. Kohout, M.J. Doble, P. Wadhams, C. Guan, H.H. Shen, Rollover of apparent wave attenuation in ice covered seas, J. Geophys. Res. 122 (2017) 8557–8566.
[42] M.H. Meylan, L.G. Bennetts, A.L. Kohout, In situ measurements and analysis of ocean waves in the Antarctic marginal ice zone, Geophys. Res. Lett. 41 (2014) 5046–5051.
[43] K. Newyear, S. Martin, A comparison of theory and laboratory measurements of wave propagation and attenuation in grease ice, J. Geophys. Res. 102 (1997) 25091–25099.
[44] P. Guyenne, E.I. Părău, Numerical simulation of solitary-wave scattering and damping in fragmented sea ice, in: Proc. 27th Intl. Ocean Polar Engng Conference, San Francisco, USA, 25–30 June 2017, pp. 373–380.
[45] E. Părău, F. Dias, Nonlinear effects in the response of a floating ice plate to a moving load, J. Fluid Mech. 460 (2002) 281–305.